Cell

The *Lin28/let-7* Axis Regulates Glucose Metabolism

Hao Zhu,[1,2,3,4,14] Ng Shyh-Chang,[1,2,8,14] Ayellet V. Segrè,[5,6] Gen Shinoda,[1,2] Samar P. Shah,[1,2] William S. Einhorn,[1,2,4] Ayumu Takeuchi,[1,2] Jesse M. Engreitz,[7] John P. Hagan,[1,2,8,9] Michael G. Kharas,[1,2,4] Achia Urbach,[1,2] James E. Thornton,[1,2,8] Robinson Triboulet,[1,2,8] Richard I. Gregory,[1,2,8] DIAGRAM Consortium,[13] MAGIC Investigators,[13] David Altshuler,[5,6,10] and George Q. Daley[1,2,4,8,11,12,*]

[1]Stem Cell Transplantation Program, Stem Cell Program, Division of Pediatric Hematology/Oncology, Children's Hospital Boston and Dana Farber Cancer Institute, Boston, MA, USA
[2]Harvard Stem Cell Institute, Boston, MA, USA
[3]Division of Medical Oncology, Dana Farber Cancer Institute, Boston, MA, USA
[4]Division of Hematology, Brigham and Women's Hospital, Boston, MA, USA
[5]Department of Molecular Biology, Diabetes Unit Department of Medicine, and Center for Human Genetics Research, Massachusetts General Hospital, Boston, MA, USA
[6]Program in Medical and Population Genetics, Broad Institute of Harvard and Massachusetts Institute of Technology, Cambridge, MA, USA
[7]Division of Health Sciences and Technology, MIT, Cambridge, MA, USA
[8]Department of Biological Chemistry and Molecular Pharmacology, Harvard Medical School, Boston, MA, USA
[9]Department of Molecular Virology, Immunology and Medical Genetics, The Ohio State University Medical Center, Columbus, OH, USA
[10]Departments of Genetics and of Medicine, Harvard Medical School, Boston, MA, USA
[11]Howard Hughes Medical Institute, Boston, MA, USA
[12]Manton Center for Orphan Disease Research, Boston, MA, USA
[13]Memberships of the consortia are provided in Text S1 available online
[14]These authors contributed equally to this work
*Correspondence: george.daley@childrens.harvard.edu
DOI 10.1016/j.cell.2011.08.033

SUMMARY

The *let-7* tumor suppressor microRNAs are known for their regulation of oncogenes, while the RNA-binding proteins *Lin28a/b* promote malignancy by inhibiting *let-7* biogenesis. We have uncovered unexpected roles for the *Lin28/let-7* pathway in regulating metabolism. When overexpressed in mice, both *Lin28a* and *LIN28B* promote an insulin-sensitized state that resists high-fat-diet induced diabetes. Conversely, muscle-specific loss of *Lin28a* or overexpression of *let-7* results in insulin resistance and impaired glucose tolerance. These phenomena occur, in part, through the *let-7*-mediated repression of multiple components of the insulin-PI3K-mTOR pathway, including *IGF1R, INSR,* and *IRS2*. In addition, the mTOR inhibitor, rapamycin, abrogates *Lin28a*-mediated insulin sensitivity and enhanced glucose uptake. Moreover, *let-7* targets are enriched for genes containing SNPs associated with type 2 diabetes and control of fasting glucose in human genome-wide association studies. These data establish the *Lin28/let-7* pathway as a central regulator of mammalian glucose metabolism.

INTRODUCTION

Metabolic disease and malignancy are proposed to share common biological mechanisms. Reprogramming toward glycolytic metabolism can increase a cancer cell's ability to generate biomass, a phenomenon termed the "Warburg Effect" (Denko, 2008; Engelman et al., 2006; Gao et al., 2009; Guertin and Sabatini, 2007; Laplante and Sabatini, 2009; Vander Heiden et al., 2009; Yun et al., 2009). Likewise, many genes identified in type 2 diabetes (T2D) genome wide association studies (GWAS) are proto-oncogenes or cell cycle regulators (Voight et al., 2010). MicroRNAs (miRNAs) are also emerging as agents of metabolic and malignant regulation in development and disease (Hyun et al., 2009; Peter, 2009). The *let-7* miRNA family members act as tumor suppressors by negatively regulating the translation of oncogenes and cell cycle regulators (Johnson et al., 2005; Lee and Dutta, 2007; Mayr et al., 2007; Kumar et al., 2008). Widespread expression and redundancy among the well-conserved *let-7* miRNAs raise the question of how cancer and embryonic cells are able to suppress this miRNA family to accommodate rapid cell proliferation. In human cancers, loss of heterozygosity, DNA methylation, and transcriptional suppression have been documented as mechanisms to reduce *let-7* (Johnson et al., 2005; Lu et al., 2007). Another mechanism for *let-7* downregulation involves the RNA-binding proteins *Lin28a* and *Lin28b* (collectively referred to as *Lin28a/b*), which are highly expressed during normal embryogenesis and upregulated in some cancers to potently and selectively block the maturation of *let-7* (Heo et al., 2008; Newman et al., 2008; Piskounova et al., 2008; Rybak et al., 2008; Viswanathan et al., 2008). By repressing the biogenesis of *let-7* miRNAs and in some cases through direct mRNA binding and enhanced translation (Polesskaya et al., 2007; Xu and Huang, 2009; Xu et al., 2009; Peng et al., 2011), *Lin28a/b* regulate an array of targets involved in cell proliferation and

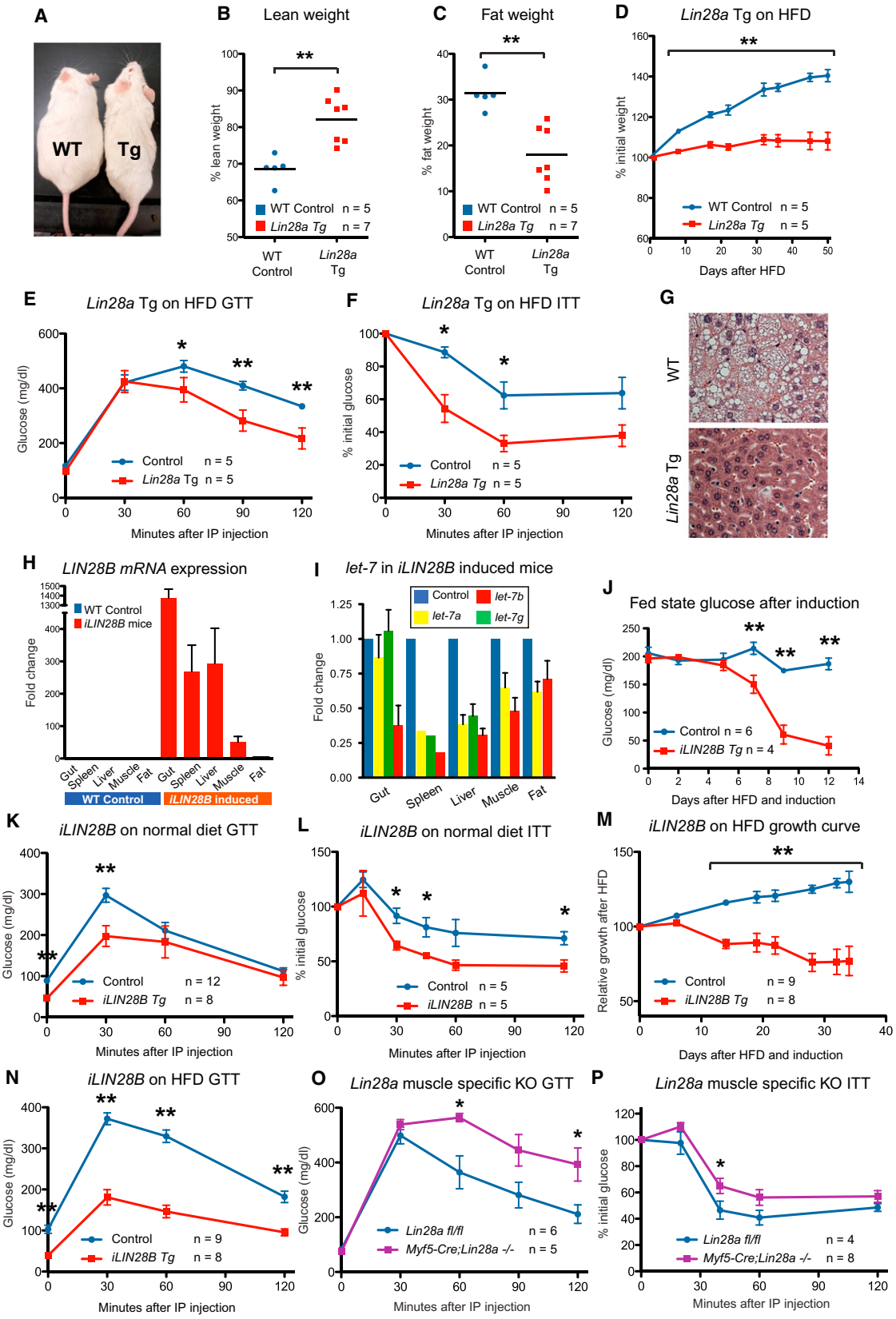
A
WT
Tg
B
Lean weight
% lean weight
WT Control n = 5
Lin28a Tg n = 7
WT Control
Lin28a Tg
C
Fat weight
% fat weight
WT Control n = 5
Lin28a Tg n = 7
D
Lin28a Tg on HFD
% initial weight
WT Control n = 5
Lin28a Tg n = 5
Days after HFD
E
Lin28a Tg on HFD GTT
Glucose (mg/dl)
Control n = 5
Lin28a Tg n = 5
Minutes after IP injection
F
Lin28a Tg on HFD ITT
% initial glucose
Control n = 5
Lin28a Tg n = 5
Minutes after IP injection
G
WT
Lin28a Tg
H
LIN28B mRNA expression
Fold change
WT Control
iLIN28B mice
Gut
Spleen
Liver
Muscle
Fat
WT Control
iLIN28B induced
I
let-7 in iLIN28B induced mice
Control
let-7b
let-7a
let-7g
Fold change
Gut
Spleen
Liver
Muscle
Fat
J
Fed state glucose after induction
Glucose (mg/dl)
Control n = 6
iLIN28B Tg n = 4
Days after HFD and induction
K
iLIN28B on normal diet GTT
Glucose (mg/dl)
Control n = 12
iLIN28B Tg n = 8
Minutes after IP injection
L
iLIN28B on normal diet ITT
% initial glucose
Control n = 5
iLIN28B n = 5
Minutes after IP injection
M
iLIN28B on HFD growth curve
Relative growth after HFD
Control n = 9
iLIN28B Tg n = 8
Days after HFD and induction
N
iLIN28B on HFD GTT
Glucose (mg/dl)
Control n = 9
iLIN28B Tg n = 8
Minutes after IP injection
O
Lin28a muscle specific KO GTT
Glucose (mg/dl)
Lin28a fl/fl n = 6
Myf5-Cre;Lin28a -/- n = 5
Minutes after IP injection
P
Lin28a muscle specific KO ITT
% initial glucose
Lin28a fl/fl n = 4
Myf5-Cre;Lin28a -/- n = 8
Minutes after IP injection

differentiation in the context of embryonic stem cells and cancer (Viswanathan and Daley, 2010).

Little is known about the in vivo function of the *Lin28/let-7* axis. The pathway was first revealed in a screen for heterochronic mutants in *C. elegans*, where loss of *lin-28* resulted in precocious vulval differentiation and premature developmental progression (Ambros and Horvitz, 1984; Moss et al., 1997; Nimmo and Slack, 2009), whereas loss of *let-7* led to reiteration of larval stages and delayed differentiation (Abbott et al., 2005; Reinhart et al., 2000). We previously showed that *Lin28a* gain of function promotes mouse growth and delays sexual maturation, recapitulating the heterochronic effects of *lin-28* and *let-7* in *C. elegans*, as well as the height and puberty phenotypes linked to human genetic variation at the *Lin28b* locus identified in GWAS (Zhu et al., 2010). The conservation of *Lin28* and *let-7's* biochemical and physiological functions throughout evolution suggests an ancient mechanism for *Lin28* and *let-7's* effects on growth and developmental timing.

In this report we found that both *Lin28a* and *LIN28B* transgenic mice were resistant to obesity and exhibited enhanced glucose tolerance. In contrast, muscle-specific *Lin28a* knockout and inducible *let-7* transgenic mice displayed glucose intolerance, suggesting that the *Lin28/let-7* pathway plays a specific and tightly regulated role in modulating glucose metabolism in mammals. In vitro experiments revealed that *Lin28a* enhances glucose uptake via an increase in insulin-PI3K-mTOR signaling due in part to the derepression of multiple direct *let-7* targets in the pathway, including *IGF1R*, *INSR*, *IRS2*, *PIK3IP1, AKT2, TSC1* and *RICTOR*. Experiments with the mTOR-specific inhibitor rapamycin demonstrate that *Lin28a* regulates growth, glucose tolerance, and insulin sensitivity in an mTOR-dependent manner in vivo. In addition, analysis of T2D and fasting glucose whole genome associations suggests a genetic connection between multiple genes regulated by *let-7* and glucose metabolism in humans. These metabolic functions for *Lin28a/b* and *let-7* in vivo provide a mechanistic explanation for how this pathway might influence embryonic growth, metabolic disease and cancer.

RESULTS

Lin28a Tg Mice Are Resistant to Obesity and Diabetes

We previously described a tetracycline-inducible *Lin28a* transgenic (*Lin28a* Tg) mouse that showed leaky constitutive *Lin28a* expression in the absence of induction (Zhu et al., 2010). In that study, we showed that these mice cleared glucose more efficiently during glucose and insulin tolerance testing (GTT and ITT), classic metabolic tests used for the characterization of whole animal glucose handling. Given that young *Lin28a* Tg mice exhibited enhanced glucose metabolism, we tested if old *Lin28a* Tg mice were also resistant to age-induced obesity. Compared to *Lin28a* Tg mice, wild-type mice fed a normal diet gained significantly more fat mass with age (Figure 1A). Dual Energy X-ray Absorptiometry scans showed increased percentage lean mass and reduced percentage body fat in the *Lin28a* Tg mice (Figures 1B and 1C). To rule out behavioral alterations, we measured activity over three days in isolation cages and found no differences in horizontal activity, O_2/CO_2 exchange, and food/water intake between wild-type and Tg mice (Figures S1A and S1B available online). To determine if these mice were resistant to HFD-induced obesity, we fed mice a diet containing 45% kcals from fat, and observed resistance to obesity in the *Lin28a* Tg mice (Figure 1D). *Lin28a* Tg mice consumed as much high-fat food as their wild-type littermates, ruling out anorexia (data not shown). Furthermore, we inquired if *Lin28a* Tg mice were resistant to HFD-induced diabetes and found that they had markedly improved glucose tolerance and insulin sensitivity under HFD conditions (Figures 1E and 1F). *Lin28a* Tg mice also showed resistance to HFD-induced hepatosteatosis (Figure 1G). Taken together, leaky *Lin28a* expression in the muscle, skin and connective tissues (Zhu et al., 2010) protected against obesity and diabetes in the context of aging and HFD.

iLIN28B Tg Mice Are Resistant to Diabetes

Although *Lin28a* and *Lin28b* both block *let-7* miRNAs, they are differentially regulated, resulting in distinct expression patterns during normal development and malignant transformation (Guo et al., 2006; Viswanathan et al., 2009). Given that *LIN28B* is overexpressed more frequently than *LIN28A* in human cancer, we sought to determine if *LIN28B* exerts a similar effect on glucose metabolism. Thus, we generated a mouse strain carrying an inducible copy of human *LIN28B* driven by a tetracycline transactivator *rtTA* placed under the control of the *Rosa26* locus (*iLIN28B* mouse, see Experimental Procedures). After 14 days of treatment with the tetracycline analog doxycycline (dox), high levels of *LIN28B* were induced and mature *let-7's* were

Figure 1. Lin28a Tg and iLIN28B Tg Mice Are Resistant to Obesity and Diabetes and Lin28a Is Physiologically Required for Normal Glucose Homeostasis

(A) Aged wild-type (left) and *Lin28a* Tg mice (right) fed a normal diet, at 20 weeks of age.
(B) Percentage body fat and (C) lean mass as measured by DEXA.
(D) Weight curve of mice fed a HFD containing 45% kcals from fat.
(E) Glucose tolerance test (GTT) and (F) Insulin tolerance test (ITT) of mice on HFD.
(G) Liver histology of mice fed HFD.
(H) Human *LIN28B* mRNA expression in a mouse strain with dox inducible transgene expression (named *iLIN28B*).
(I) Mature *let-7* expression in gut, spleen, liver, muscle and fat.
(J) Kinetics of fed state glucose change after induction.
(K) GTT and (L) ITT under normal diets.
(M) *iLIN28B* growth curve under HFD.
(N) GTT after 14 days of HFD and induction.
(O) GTT and (P) ITT of *Myf5-Cre; Lin28a*$^{fl/fl}$ mouse.
Controls for *Lin28a* Tg mice are WT. Controls for *iLIN28B* Tg mice carry only the *LIN28B* transgene. Controls for muscle knockout mice are *Lin28a*$^{fl/fl}$ mice. The numbers of experimental animals are listed within the charts. Error bars represent SEM. *$p < 0.05$, **$p < 0.01$.

repressed in metabolically important organs (Figures 1H and 1I), resulting in hypoglycemia with an average fasting glucose of < 50 mg/dL in induced mice compared to > 150 mg/dL in control mice ($p < 0.01$). To determine the kinetics of this effect, we measured fed state glucose daily and noted falling glucose levels after 5 days (Figure 1J). Glucose and insulin tolerance tests on dox-induced animals on normal diets showed considerable improvements in glucose tolerance and insulin sensitivity (Figures 1K and 1L). When assessing islet β cell hyperactivity, we found that *iLIN28B* mice produced no more insulin than control littermates during glucose challenge (data not shown). Under HFD, we found that induced *iLIN28B* mice were surprisingly resistant to weight gain (Figure 1M) despite a trend toward increased food intake (9.9 versus 4.8 g/mouse/day; $p = 0.075$). These mice continued to exhibit superior glucose tolerance after 14 days of dox induction under HFD (Figure 1N), when average weights were 34.5 ± 1.05 g for controls and 27.1 ± 0.99 g for *iLIN28B* mice, demonstrating that HFD had a strong obesogenic and diabetogenic effect on control but not on *LIN28B* induced animals. Unlike the *Lin28a* Tg mice, expression was not leaky in the *iLIN28B* mice (Figure 1H and 3F) and uninduced mice exhibited no growth or glucose phenotypes (Figures S1C and S1D), making this a better model for inducible *Lin28* hyperactivation. These data show that both *Lin28* homologs have similar effects on glucose metabolism and obesity, suggesting that these effects are mediated through common mRNA or miRNA targets of the *Lin28* family.

Lin28a Is Physiologically Required for Normal Glucose Homeostasis

We then asked if *Lin28a* is physiologically required for normal glucose metabolism in one specific adult tissue compartment, skeletal muscle, since previous studies have found low but significant levels of *Lin28a* expression in the muscle tissues of mice (Yang and Moss, 2003; Zhu et al., 2010). We generated a skeletal muscle-specific knockout of *Lin28a* (see Experimental Procedures). These muscle-specific knockout mice showed impaired glucose tolerance (Figure 1O) and insulin resistance (Figure 1P) relative to wild-type littermates, demonstrating that *Lin28a* activity in skeletal muscles is required for normal glucose homeostasis. We analyzed miRNA expression in muscle tissue by qRT-PCR and found no significant difference in *let-7* levels during adult (data not shown) or embryonic stages (Figure S1E), suggesting that *Lin28a* loss of function affects glucose homeostasis either through *let-7*-independent mRNA binding or through changes in the spatiotemporal distribution of *let-7* miRNA. Together, these data show that *Lin28* isoforms are important and essential regulators of glucose homeostasis.

iLet-7 Mice Are Glucose Intolerant

In addition to their ability to suppress *let-7* biogenesis, *Lin28a* and *Lin28b* also regulate mRNA targets such as *Igf2*, *HMGA1, OCT4*, histones and cyclins through non-*let-7* dependent mechanisms of mRNA binding and enhanced translation (Polesskaya et al., 2007; Xu and Huang, 2009; Xu et al., 2009; Peng et al., 2011). To test if altered *let-7* expression might produce the opposite phenotypes of *Lin28a/b* gain of function, we generated a mouse strain in which *let-7g* can be induced with dox under the control of the *Rosa26* locus (*iLet-7* mouse, See Experimental Procedures). To ensure that endogenous *Lin28* would not block *pri- or pre-let-7g* biogenesis, we used a chimeric *let-7g* species called *let-7S21L* (*let-7g* Stem, *mir-21 Loop*), in which the loop region of the precursor miRNA derives from *mir-21* and cannot be bound by *Lin28*, thus allowing for *let-7* processing despite *Lin28* expression (Piskounova et al., 2008). Global transgene induction from three weeks of age onward increases mature *let-7g* levels in liver (>50-fold), skin (>20-fold), fat (~4-fold) and muscle (~4-fold) (Figure 2A). This level of *let-7* overexpression led to reduced body size and growth rates in induced animals (Figures 2B and 2C). Growth retardation was proportional and not manifested as preferential size reduction in any particular organs (Figure S2A). Similar to the *iLIN28B* mice, leaky expression was not detected and uninduced male mice exhibited no growth or glucose phenotypes (Figures S2B–S2D).

After 5 days of *let-7* induction, these *iLet-7* mice produced an increase in fed state glucose (Figure 2D). GTT revealed glucose intolerance in mice fed normal (Figure 2E) or HFD (Figure 2F). Surprisingly, ITT failed to detect a difference in insulin sensitivity (Figure 2G). The decreased glucose tolerance in the setting of comparable insulin sensitivity suggested either decreased insulin production from islet β cells in response to glucose, or higher insulin secretion to compensate for peripheral insulin resistance. Thus, we measured insulin production following glucose challenge, and found that *iLet-7* mice produced more insulin than controls (Figure 2H). These results demonstrated that broad overexpression of *let-7* results in peripheral glucose intolerance and compensatory overproduction of insulin from islet β cells.

To test if *let-7* induction could abrogate the glucose uptake phenotype of *LIN28B* overexpression, we crossed the *iLIN28B* to the *iLet-7* inducible mice. After 10 days of induction, simultaneous induction of *LIN28B* and *let-7g* did not result in any differences in glucose tolerance (Figures 2I and 2J), in contrast to *LIN28B* or *let-7g* induction alone. Taken together, the opposing effects of *Lin28* and *let-7* expression on glucose regulation show that *Lin28* overexpression influences metabolism in part by suppressing *let-7*, and that *let-7* alone is sufficient to regulate glucose metabolism in vivo.

Insulin-PI3K-mTOR Signaling Is Activated by *Lin28a/b* and Suppressed by *let-7*

To dissect the molecular mechanism of the effects of *Lin28* and *let-7* on glucose regulation, we turned to the C2C12 cell culture system. Overexpression of *Lin28a* in C2C12 myoblasts resulted in protein levels of *Lin28a* similar to that observed in mouse embryonic stem cells (ESCs) (Figure 3A), and led to robust *let-7* suppression (Figure 3B). In C2C12 myotubes differentiated for 3 days, *Lin28a* promoted Ser473 phosphorylation of Akt and Ser235/236 phosphorylation of S6 ribosomal protein, suggesting activation of the PI3K-mTOR pathway (Figure S3A). In this setting, *Lin28a* increased myotube glucose uptake by 50% (Figure 3C). *Lin28a*-dependent glucose uptake was abrogated by 24hr treatment with the PI3K/mTOR inhibitor LY294002 or the mTOR inhibitor rapamycin (Figure 3C), but not the MAPK/ERK inhibitor PD98059 (Figure S3B), demonstrating that *Lin28a*-dependent glucose uptake requires the PI3K-mTOR pathway.

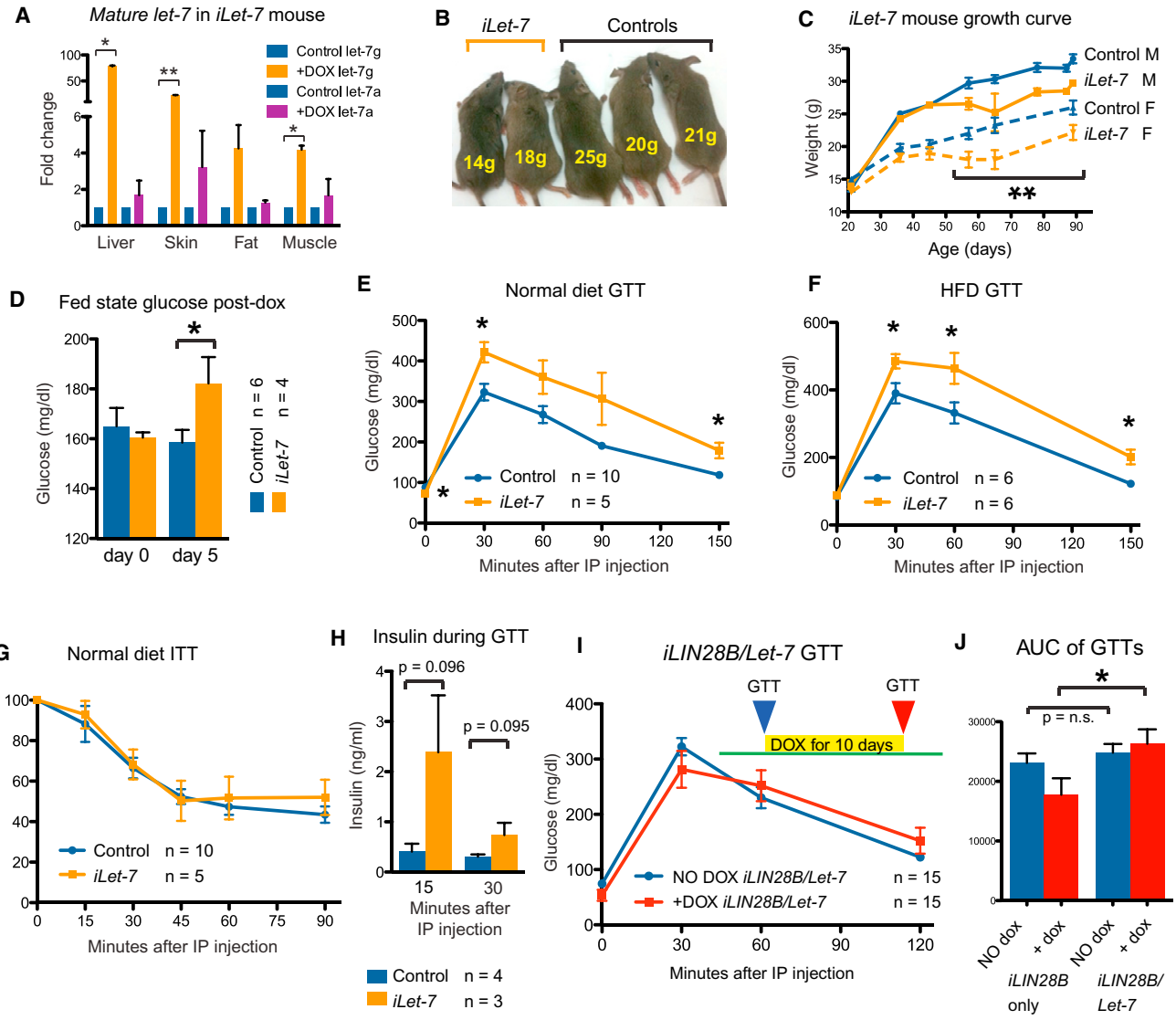

Figure 2. *iLet-7* Mice Are Glucose Intolerant

(A) *let-7g* and *let-7a* qRT-PCR in tissues of dox induced *iLet-7* mice (n = 3) and controls (n = 3).

(B) Reduced size of induced animals.

(C) *iLet-7* growth curve for males and females.

(D) Fed state glucose in *iLet-7* mice induced for 5 days.

GTTs performed on mice fed with either (E) normal diet or (F) HFD.

(G) ITT on normal diet.

(H) Insulin production during a glucose challenge.

(I) GTT of *LIN28B/Let-7* compound heterozygote mice before (blue) and after (red) induction with dox.

(J) Area under the curve (AUC) analysis for this GTT.

Controls for *iLet-7* Tg mice carry either the *Let-7* or *Rosa26-M2rtTa* transgene only. The numbers of experimental animals are listed within the charts. Error bars represent SEM. *p < 0.05, **p < 0.01.

To exclude myotube differentiation-dependent phenomena, we tested the effects of *Lin28a* on PI3K-mTOR signaling in undifferentiated myoblasts under serum-fed, serum-starved, and insulin-stimulated conditions (Figure 3D). In the serum-fed state, we found that *Lin28a* promoted the activation of PI3K/Akt signaling by increasing Akt phosphorylation at both Ser473 and Thr308, compared to the pBabe control. Furthermore, we found that *Lin28a* robustly increased the phosphorylation of mTORC1 signaling targets S6 and 4EBP1 in the serum-fed state. Serum-starvation for 18 hr abrogated the phosphorylation of Akt, S6 and 4EBP1, indicating that *Lin28a*-induction of PI3K-mTOR signaling requires exogenous growth factor stimulation. Upon insulin stimulation, Akt phosphorylation increased dramatically and, both phospho-S6 and phospho-4EBP1 levels were

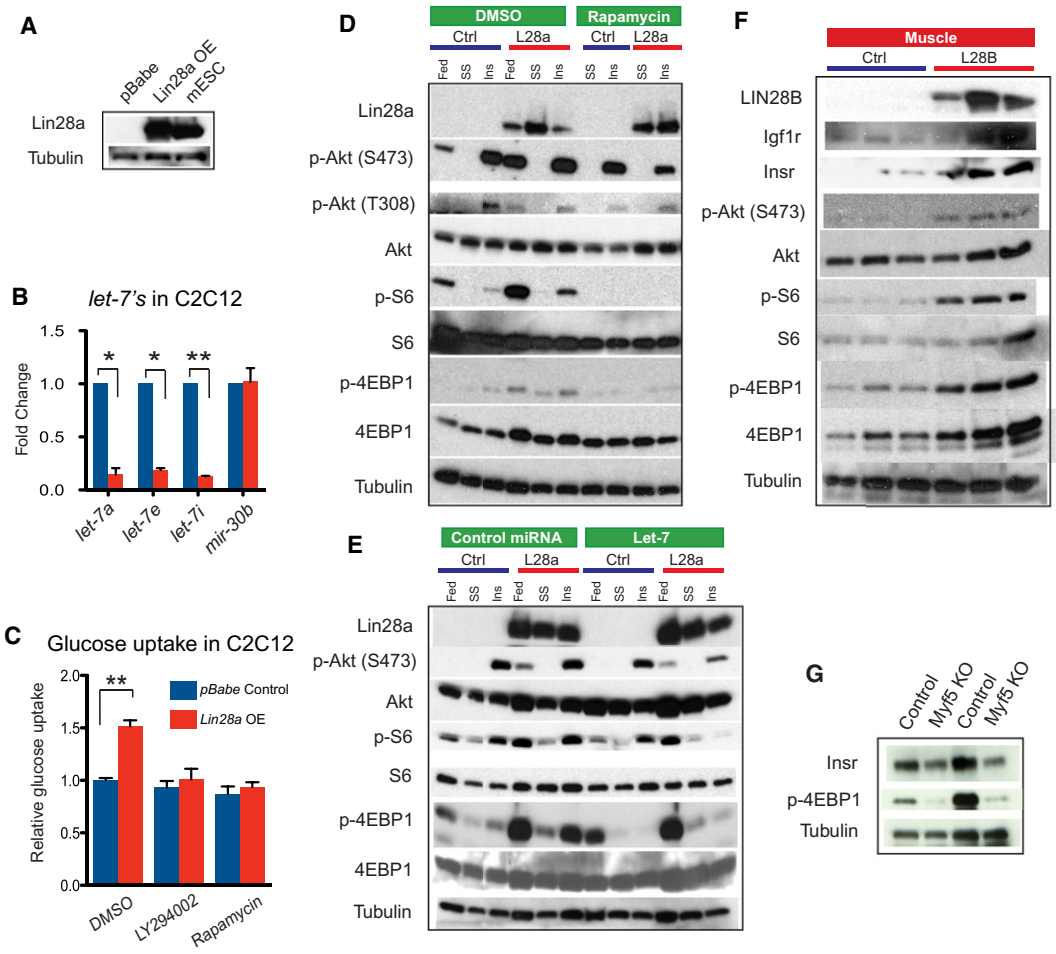

Figure 3. Insulin-PI3K-mTOR Signaling Is Activated by *Lin28a/b* and Suppressed by *let-7*

(A) Western blot analysis of Lin28a protein expression in C2C12 myoblasts infected with control pBabe or *Lin28a* overexpression vector, and mouse ESCs, with tubulin as the loading control.

(B) Quantitative PCR for *let-7* isoforms in C2C12 myoblasts, normalized to *sno142*, after *Lin28a* overexpression.

(C) 2-deoxy-D-[^{3}H] glucose uptake assay on 3-day-differentiated C2C12 myotubes with and without *Lin28a* overexpression, treated with DMSO, the PI3K inhibitor LY294002, and the mTOR inhibitor rapamycin for 24 hr.

(D) Western blot analysis of the effects of *Lin28a* overexpression on PI3K-mTOR signaling in C2C12 myoblasts, under serum-fed (fed), 18 hr serum starved (SS) or insulin-stimulated (Ins) conditions. Insulin stimulation was performed in serum-starved myoblasts with 10 μg/mL insulin for 5 min. Prior to insulin stimulation, serum-starved myoblasts were treated with either DMSO or 20 ng/mL rapamycin for 1 hr.

(E) Western blot analysis of the effects of *let-7f* or control miRNA on PI3K-mTOR signaling in C2C12 myoblasts under serum-fed (fed), 18 hr serum starved (SS) or insulin-stimulated (Ins) conditions.

(F) Western blot analysis of the effects of *LIN28B* induction by dox on PI3K-mTOR signaling in quadriceps muscles in vivo (n = 3 *iLIN28B* Tg mice and 3 *LIN28B* Tg only mice).

(G) Insr and p-4EBP1 protein levels in wild-type and *Lin28a* muscle-specific knockout adults. Error bars represent SEM. *$p < 0.05$, **$p < 0.01$.

increased even further by *Lin28a* overexpression, suggesting that *Lin28a* increases the insulin-sensitivity of C2C12 myoblasts. Importantly, we found that rapamycin abrogated the *Lin28a*-induction of phospho-S6 and phospho-4EBP1 upon insulin stimulation, but did not affect *let-7* levels (Figure S3C) or Lin28a itself (Figure 3D), indicating that the mTOR dependence is occurring downstream of *Lin28a*.

To test if the effects of *Lin28a* on insulin-PI3K-mTOR signaling are *let-7*-dependent, we transfected either mature *let-7f* duplex or a negative control miRNA into both *Lin28a*-overexpressing and pBabe control myoblasts (Figure S3D and Figure 3E). Because mature *let-7* duplexes cannot be bound and inhibited by Lin28a protein, this experiment tests if PI3K-mTOR activation is occurring downstream of *let-7*. Transfection with control miRNA did not affect *Lin28a*-induction of the phosphorylation of Akt, S6, or 4EBP1 in serum-starved myoblasts upon insulin stimulation. Transfection with *let-7f,* however, attenuated the *Lin28a*-induction of phospho-Akt (Ser473), and abrogated the increase in S6 and 4EBP1 phosphorylation upon insulin stimulation in *Lin28a*-overexpressing myoblasts (Figure 3E). In pBabe control myoblasts, *let-7* duplex still suppressed S6 and 4EBP1 phosphorylation in the serum-fed state, serum-starved, and

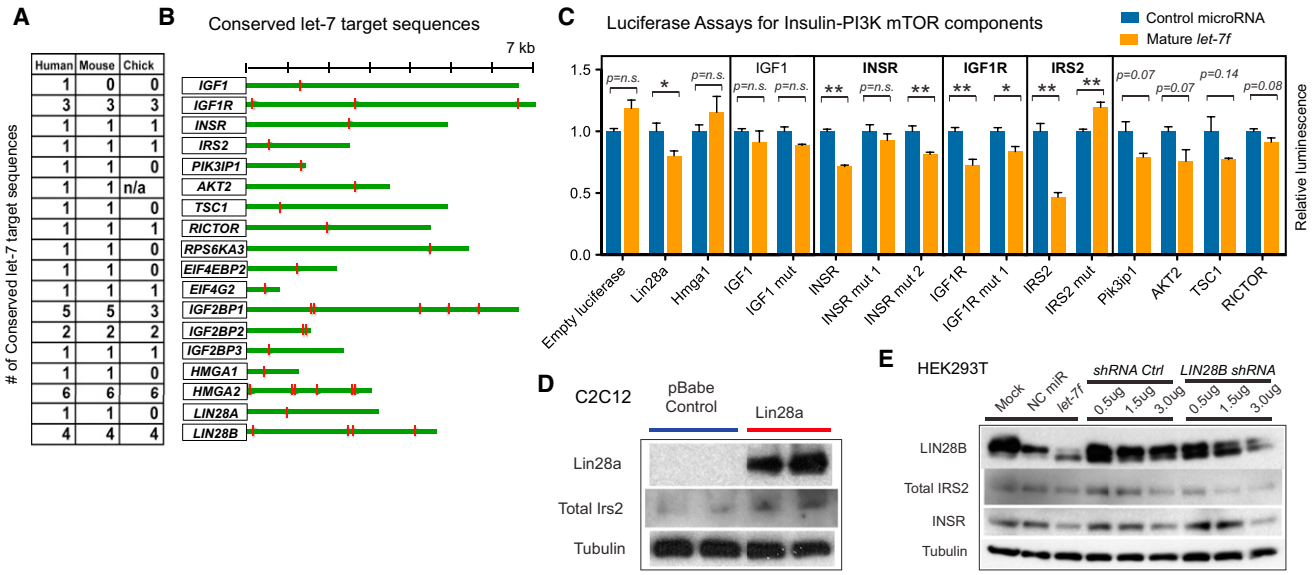

Figure 4. *Lin28a/b* and *let-7* Regulate Genes in the Insulin-PI3K-mTOR Pathway

(A) Shown are the numbers of conserved *let-7* binding sites within 3′UTRs found using the TargetScan algorithm.

(B) Putative *let-7* binding sites in 16 genes of the insulin-PI3K-mTOR pathway and in *Lin28a/b*.

(C) 3′UTR luciferase reporter assays performed to determine functional *let-7* binding sites. Bar graphs show relative luciferase reporter expression in human HEK293T cells after transfection of mature *let-7f* duplex normalized to negative control miRNA. Shown also are mutations in the seed sequence of the *let-7* binding sites for *INSR*, *IGF1R* and *IRS2*.

(D) Western blot analysis of Lin28a, Irs2, and tubulin in C2C12 myoblasts with and without Lin28a overexpression.

(E) Western blot analysis of LIN28B, total IRS2, INSR and TUBULIN in HEK293T cells with either *let-7f* transfection or shRNA knockdown of *LIN28B*. Error bars represent SEM. *p < 0.05, **p < 0.01.

insulin-stimulated conditions, relative to total S6 and 4EBP1 protein. The suppression of mTOR signaling by *let-7* even in the absence of *Lin28a* implies that *let-7* can act independently downstream of *Lin28a.* Together with data indicating that *let-7* abrogates *Lin28a*-specific induction of p-Akt, p-S6 and p-4EBP1 upon insulin stimulation, this demonstrates that the effects of *Lin28a* on PI3K-mTOR signaling are at least in part due to *let-7* and that *Lin28* and *let-7* exert opposing effects on PI3K-mTOR signaling.

To test if these effects of *Lin28* on insulin-PI3K-mTOR signaling are also relevant in vivo, we examined the quadriceps muscles of *iLIN28B* mice and found that dox-induction led to increases in the phosphorylation of Akt (S473), S6 and 4EBP1, the targets of PI3K-mTOR signaling (Figure 3F). Furthermore, the Insulin-like growth factor 1 receptor (Igf1r) and the Insulin receptor (Insr) proteins were also upregulated in the muscles upon *LIN28B* induction, reinforcing the fact that *Lin28a/b* drives insulin-PI3K-mTOR signaling in C2C12 myoblasts and within mouse tissues. On the other hand, similar analysis of the *Lin28a* muscle-specific knockout mice revealed reduced Insr and p-4EBP1 expression (Figure 3G), demonstrating that *Lin28a* is both necessary and sufficient to influence glucose metabolism through the regulation of insulin-PI3K-mTOR signaling in vivo.

Lin28a/b and *let-7* Regulate Genes in the Insulin-PI3K-mTOR Pathway

On the RNA level, *Lin28a* overexpression in C2C12 myoblasts leads to an increase in mRNA levels of multiple genes in the insulin-PI3K-mTOR signaling pathway (Figure S4A). Although both *Lin28a* suppression of *let-7* and direct *Lin28a* binding to mRNAs could increase mRNA stability and thus increase mRNA levels, it is possible that these increases do not reflect direct interactions. To find direct targets, we performed a bioinformatic screen using the TargetScan 5.1 algorithm (Grimson et al., 2007), and found that 16 genes in the insulin-PI3K-mTOR pathway contained evolutionarily conserved *let-7* binding sites in their respective 3′UTRs (Figures 4A and 4B). Next, we performed 3′ UTR luciferase reporter assays to determine if these genes were bona fide and direct targets of *let-7*. To do this, we generated luciferase reporters with twelve human 3′UTR fragments containing conserved *let-7* sites. Luciferase reporter expression in human HEK293T cells after transfection of either mature *let-7f* duplex or a negative control miRNA demonstrated that the 3′ UTRs of *INSR, IGF1R, IRS2*, *PIK3IP1, AKT2, TSC1* and *RICTOR* were targeted by *let-7* for suppression (Figure 4C). Three-base mismatch mutations in the seed region of the *let-7* binding sites abrogated *let-7*'s suppression of *INSR*, *IGF1R* and *IRS2*. To confirm that the luciferase reporters predicted actual changes in protein expression mediated by *let-7*, we assayed the endogenous expression of some of these proteins upon *Lin28a/b* overexpression. We found that an increase in *Lin28a* upregulated Irs2 (Figure 4D) in vitro, and that an increase in *LIN28B* upregulated Igf1r and Insr protein in skeletal muscles in vivo (Figure 3F). Conversely, INSR and IRS2 are reduced upon both *let-7f* transfection and *LIN28B* shRNA knockdown in HEK293T, demonstrating that these

regulatory mechanisms hold in both mouse and human cells, and in the setting of both LIN28B gain and loss of function (Figure 4E). This establishes a direct mechanism for *let-7*'s repression and *Lin28*'s derepression of multiple components in the insulin-PI3K-mTOR signaling cascade.

Previously, *Lin28a* has been shown to enhance *Igf2* translation independently of *let-7* (Polesskaya et al., 2007), offering an alternative mechanism by which *Lin28a* might activate the insulin-PI3K-mTOR pathway. To determine the relative contribution of this mechanism, we performed in vitro and in vivo loss of function experiments. Following siRNA knockdown of *Igf2* in C2C12 (the efficacy of knockdown is shown in Figure S4B), we found only minimal changes in S6 and 4EBP1 phosphorylation (Figure S4C). In these C2C12 myotubes, glucose uptake was unaffected by *Igf2* knockdown, but significantly decreased by *let-7a* (Figure S4D). In addition, we crossed the *Lin28a* Tg mice with *Igf2* knockout mice and found that the absence of *Igf2* did not abrogate enhanced glucose uptake, insulin sensitivity, or the anti-obesity effect mediated by *Lin28a* (Figure S4E–H). Taken together, these data indicate that the metabolic phenotypes we have observed are not solely due to the ability of Lin28a/b to promote translation of *Igf2* mRNA, but do not rule out the possibility that Lin28a/b might modulate other mRNAs in the insulin-PI3K-mTOR signaling pathway.

mTOR Mediates *Lin28a*'s Enhancement of Growth and Glucose Metabolism In Vivo

Given that *Lin28a* activates the insulin-PI3K-mTOR pathway both in vitro and in vivo, we asked whether the metabolic effects of *Lin28a in vivo* could be abrogated by pharmacological inhibition of the mTOR pathway. To do this, we injected *Lin28a* Tg and wild-type littermates with rapamycin 3 times per week beginning when mice were 18 days old. Rapamycin abrogated the growth enhancement in *Lin28a* Tg mice at doses that had minimal growth suppressive effects on wild-type mice (Figures 5A and 5B), suggesting that *Lin28a* promotes growth in an mTOR-dependent manner. Selective suppression of *Lin28a*-driven growth was observed using several parameters: weight (Figures 5B and 5C), crown-rump length (Figure 5D), and tail width (Figure 5E). We also tested if the enhanced glucose uptake phenotype in vivo was likewise dependent on mTOR. Indeed, glucose tolerance testing showed that short-term rapamycin reversed the enhanced glucose uptake effect of *Lin28a* (Figures 5F and 5G) and reduced the insulin-sensitivity of *Lin28a* Tg mice to wild-type levels (Figures 5H and 5I). These data indicate that the glucose uptake, insulin sensitivity and animal growth phenotypes of *Lin28a* overexpression in vivo are dependent on mTOR signaling.

let-7 Target Genes Are Associated with Type 2 Diabetes in Human GWAS

Finally, we sought to assess the relevance of the *Lin28/let-7* pathway to human disease and metabolism, using human genetic studies of T2D and fasting glucose levels. Because the *Lin28/let-7* pathway has not been previously implicated in T2D, we first asked whether any of the genes that lie in T2D association regions identified in T2D GWAS and meta-analyses (Voight et al., 2010) are known or predicted *let-7* targets. We used TargetScan 5.1 to computationally predict *let-7* targets (Grimson et al., 2007), and found that 14 predicted *let-7* target genes lie in linkage disequilibrium to 39 validated common variant associations with T2D, including *IGF2BP2*, *HMGA2*, *KCNJ11* and *DUSP9* (strength of T2D association signals $p < 4 \times 10^{-9}$) (Table 1). Of the computationally predicted *let-7* targets associated with T2D, *IGF2BP1/2/3* and *Hmga2* have been verified as *let-7* targets in several studies (Boyerinas et al., 2008; Mayr et al., 2007). To validate the connection between *Lin28* and GWAS candidate genes, we analyzed the expression of *Igf2bp* and *Hmga* family members in C2C12 cells with and without *Lin28a* overexpression, and observed increases in *Igf2bp1*, *Igf2bp2*, and *Hmga2* mRNA following *Lin28a* overexpression (Figure 6A). To ensure that this was not a C2C12- or muscle-specific phenomenon, we confirmed the upregulation of these genes in 3T3 cells following human *LIN28A or LIN28B* overexpression on the mRNA (Figure 6B) and the protein level for the Igf2bp family (Figure 6C). We also observed increased expression of *Igf2bp2* and *Igf2bp3* (Figure 6D) in *Lin28a* Tg muscle, confirming this link in vivo.

We next asked whether there is a more widespread connection between T2D susceptibility and *let-7* targets, in addition to the targets in validated T2D association regions ($p < 5 \times 10^{-8}$). To address this, we applied a computational method called MAGENTA (Meta-Analysis Gene-set Enrichment of variaNT Associations) (Segrè et al., 2010) to GWAS meta-analyses of T2D and fasting glucose blood levels, and tested whether the distributions of disease or trait associations in predefined *let-7* target gene sets are skewed toward highly ranked associations (including ones not yet reaching a level of genome-wide significance) compared to matched gene sets randomly sampled from the genome (Table 1). We tested three types of *let-7* target definitions with increasing levels of target validation, from *in silico* predicted *let-7* targets using TargetScan 5.1 (Grimson et al., 2007) to experimentally defined targets. For the latter, we used (i) a set of genes with at least one *let-7* site in their 3′ UTR and whose mRNA was downregulated by *let-7b* overexpression in primary human fibroblasts (Legesse-Miller et al., 2009), and (ii) a set of genes whose protein levels were most strongly downregulated by *let-7b* overexpression in HeLa cells (Selbach et al., 2008). We first tested the *let-7* target sets against the latest T2D meta-analysis of eight GWAS (called DIAGRAM+) (Voight et al., 2010), and found significant enrichment (Table 1). The enrichment rose from 1.05-fold for the broadest definition of *let-7* targets predicted using TargetScan (~1800 genes; $p = 0.036$) to 1.92-fold for the experimentally validated target set based on protein level changes in response to *let-7* overexpression (~100 genes; $p = 1 \times 10^{-6}$). In the latter case, an excess of about 20 genes regulated by *let-7* at the protein level are predicted to contain novel SNP associations with T2D. Notably *IGF2BP2*, which is a canonical *let-7* target that lies in a validated T2D association locus, was found in all types of *let-7* target definitions in Table 1. Furthermore, the genes driving the T2D enrichment signals for the different *let-7* target sets include both functionally redundant homologs of T2D-associated genes, such as *IGF2BP1 (IGF2BP2), HMGA1 (HMGA2), DUSP12* and *DUSP16 (DUSP9)*, and genes in the insulin-PI3K-mTOR pathway, including *IRS2, INSR, AKT2* and *TSC1* (best local SNP association $p = 10^{-4}$ to $4*10^{-3}$).

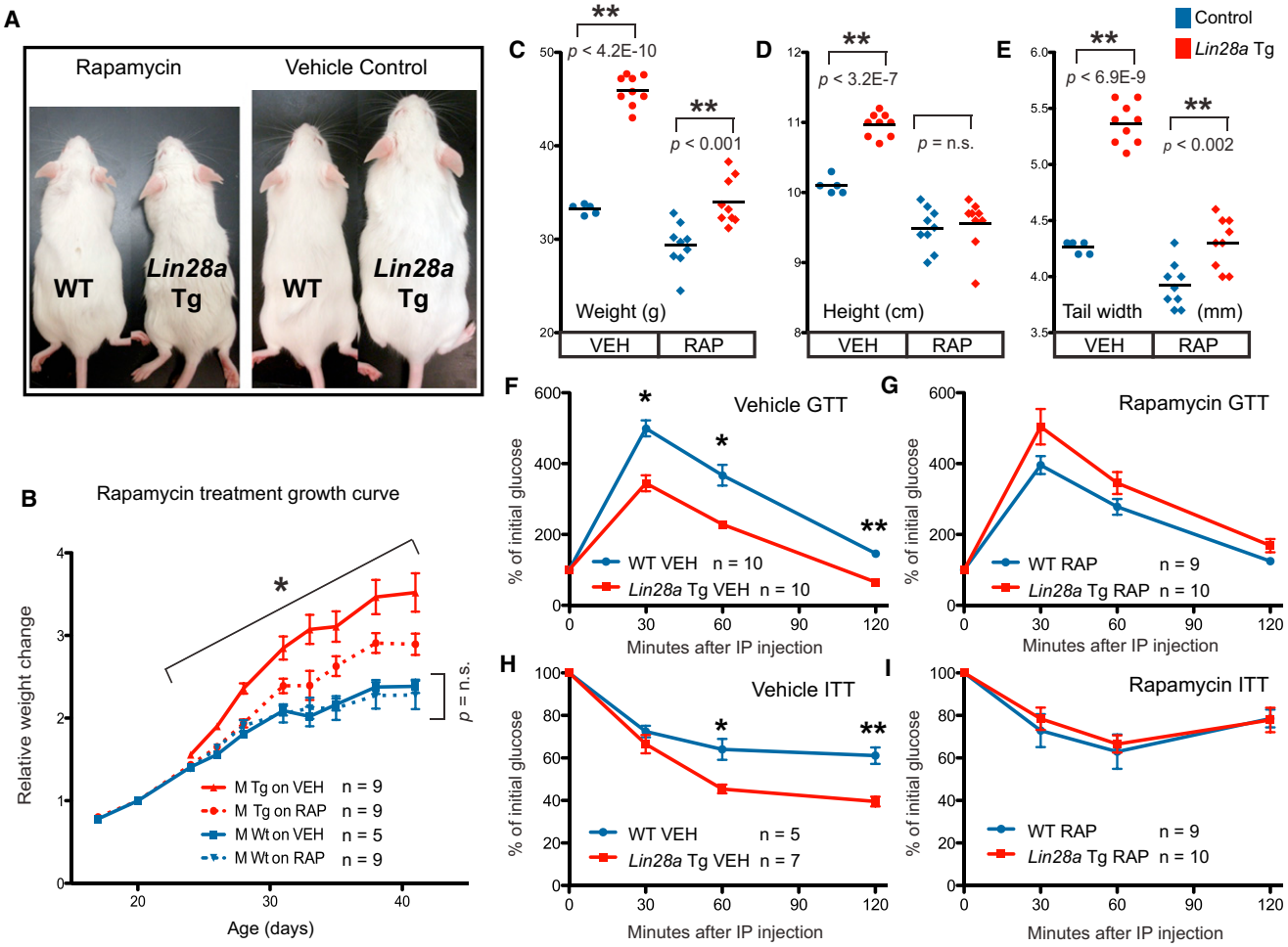

Figure 5. mTOR Is Required for *Lin28a*'s Effects on Growth and Glucose Metabolism In Vivo

(A) Rapamycin (left 2 mice) and vehicle (right 2 mice) treated wild-type and *Lin28a* Tg mice shows relative size differences.

(B) Curves showing relative growth (normalized to weight on first day of treatment) for mice treated from 3 weeks to 6.5 weeks of age. Blue and red represent wild-type and *Lin28a* Tg mice, respectively. Solid and dotted lines represent vehicle and rapamycin treated mice, respectively. Growth was measured by several other parameters:

(C) weight, (D) crown-rump length or height, and (E) tail width.

(F) GTT performed after 2 doses of vehicle or (G) rapamycin.

(H) ITT performed after 1 dose of vehicle or (I) rapamycin.

Controls for *Lin28a* Tg mice are WT. The numbers of experimental animals are listed within the charts. Error bars represent SEM. *p < 0.05, **p < 0.01.

We next tested for enrichment of *let-7* target gene associations with fasting glucose levels, using data from the MAGIC (Meta-Analysis of Glucose and Insulin-related traits Consortium) study of fasting glucose levels (Dupuis et al., 2010). We observed an over-representation of multiple genes modestly associated with fasting glucose at different levels of significance for the different *let-7* target gene sets (Table 1). The strongest enrichment was found in the genes downregulated at the mRNA level by *let-7*, an enrichment of 1.20 fold over expectation ($p = 1*10^{-4}$). Taken together, our human genetic results support the hypothesis that genes regulated by *let-7* influence human metabolic disease and glucose metabolism.

Recently it has also become clear that Lin28a/b has important *let-7*-independent roles in RNA metabolism, as evidenced by numerous direct mRNA targets whose translation is enhanced by LIN28A (Peng et al., 2011). Using GSEA, we found that this list of direct mRNA targets is also significantly enriched for glucose, insulin and diabetes-related genes (Table S1). Thus, Lin28a/b may regulate metabolism through direct mRNA-binding as well as *let-7* targets.

DISCUSSION

Lin28 and *let-7* Are Mutually Antagonistic Regulators of Growth and Metabolism

Our work defines a new mechanism of RNA-mediated metabolic regulation. In mice, *Lin28a* and *LIN28B* overexpression results in insulin sensitivity, enhanced glucose tolerance, and resistance

Table 1. MAGENTA Analysis of T2D and Fasting Glucose Associations in Different *let-7* Target Gene Set Definitions

let-7 Target Gene Set	Number of Genes Analyzed†	Nominal Gene Set Enrichment p Value	Expected Number of Genes above Enrichment Cutoff	Observed Number of Genes above Enrichment Cutoff	Enrichment Fold	Number of Genes Linked to Validated GWAS SNPs	Genes Linked to Validated GWAS SNPs
Type 2 Diabetes (DIAGRAM+ Meta-Analysis)							
All targets predicted by *TargetScan*	1763	0.036	441	462	1.05	14	*IGF2BP2*, *DUSP9*, *SLC5A6*, *TP53INP1*, *YKT6*, *ZNF512*, *HMGA2*, *KCNJ11*, *MAN2A2*, *MEST*, *NOTCH2*, *ZNF275*, *FAM72B*, *RCCD1*
Conserved targets predicted by *TargetScan*	789	0.089	197	212	1.08	7	*IGF2BP2*, *DUSP9*, *SLC5A6*, *HMGA2*, *KCNJ11*, *MAN2A2*, *ZNF275*
Downregulated mRNAs following *let-7* OE	795	0.055	199	216	1.09	9	*IGF2BP2*, *DUSP9*, *SLC5A6*, *TP53INP1*, *YKT6*, *ZNF512*, *HHEX*, *IRS1*, *TLE4*
Downregulated mRNAs following *let-7* OE + *TargetScan*	502	0.061	126	140	1.11	6	*IGF2BP2*, *DUSP9*, *SLC5A6*, *TP53INP1*, *YKT6*, *ZNF512*
Downregulated proteins following *let-7* OE	97	1.0E-06*	24	46	1.92	2	*IGF2BP2*, *CDKAL1*
Downregulated proteins following *let-7* OE + *TargetScan*	37	0.011	9	16	1.78	1	*IGF2BP2*
Fasting Glucose (MAGIC Meta-Analysis)							
All targets predicted by *TargetScan*	1708	0.015	427	450	1.05	3	*CRY2*, *SLC2A2*, *GLIS3*
Conserved targets predicted by *TargetScan*	759	0.042	190	207	1.09	1	*CRY2*
Downregulated mRNAs following *let-7* OE	750	1.0E-04*	188	226	1.20	2	*CRY2*, *FADS1*
Downregulated mRNAs following *let-7* OE + *TargetScan*	484	0.013	121	141	1.17	1	*CRY2*
Downregulated proteins following *let-7* OE	96	0.632	24	23	0.96	0	-
Downregulated proteins following *let-7* OE + *TargetScan*	35	0.245	9	11	1.22	0	-

The statistical enrichment for genes associated with T2D and fasting glucose among *let-7* targets using the MAGENTA algorithm. The TargetScan algorithm was used to define the "All human *let-7* targets" and the "Conserved *let-7* targets" gene sets (http://www.targetscan.org/). mRNA downregulation following *let-7* overexpression (OE) was measured in primary human fibroblasts (Legesse-Miller et al., 2009), and protein downregulation following *let-7* OE was measured in HeLa cells (Selbach et al., 2008). The enrichment cutoff used is the 75th percentile of all gene association scores in the genome. The enrichment fold is the ratio between the observed and expected number of genes above the enrichment cutoff. Genes linked to validated GWAS SNPs (39 SNPs for T2D and 14 SNPs for fasting glucose) were ordered according to the number of target gene sets they appear in and then alphabetically. † The following genes were removed from the analysis: (i) genes absent from the full human gene list used in the analysis, (ii) genes that had no SNPs within 110 kb upstream or 40 kb downstream to their most extreme transcript boundaries, or (iii) to correct for potential inflation of enrichment due to physical proximity of *let-7* target genes along the genome, subsets of proximal genes assigned the same best local SNP were collapsed to one gene and assigned the score of the most significant gene *p*-value in that subset. *gene sets that pass a Bonferroni corrected cutoff ($p < 0.004$).

to diabetes. Our analysis of *iLet-7* Tg mice shows that *let-7* upregulation is also sufficient to inhibit normal glucose metabolism, supporting the idea that gain of *Lin28a/b* exerts effects on whole animal glucose metabolism at least in part through *let-7* suppression. Previously, we showed that transgenic overexpression of *Lin28a* causes enhanced growth and delayed puberty, phenotypes that mimicked human traits linked to genetic variation in the *Lin28/let-7* pathway in GWAS (Zhu

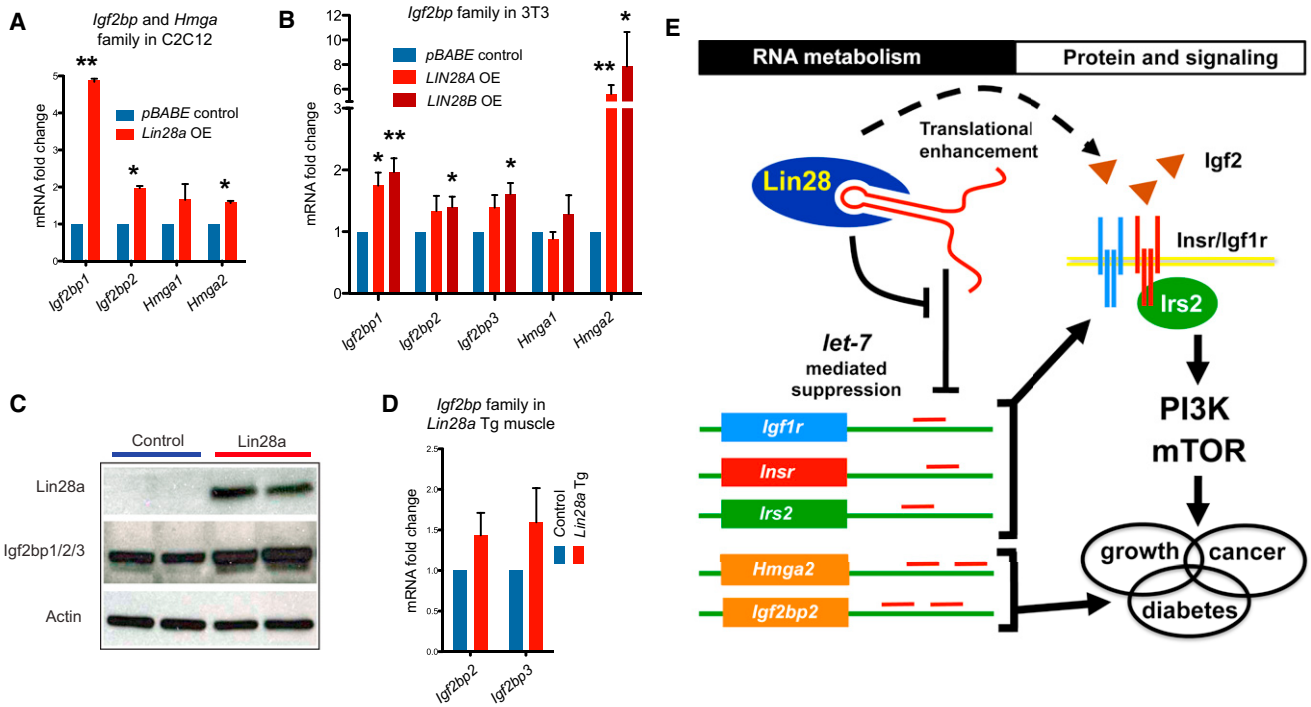

Figure 6. *let-7* Target Genes Are Associated with Type 2 Diabetes Mellitus and a Model of the *Lin28*/*let-7* Pathway in Glucose Metabolism

mRNA expression of *Igf2bp* and *Hmga* family members in (A) C2C12 with and without *Lin28a* overexpression and in (B) 3T3 cells with and without *LIN28A or LIN28B* overexpression.

(C) Western blot of NIH 3T3 cells with Lin28a overexpression showing Lin28a and Igf2bp1/2/3 protein levels (n = 3 biological replicates).

(D) *Igf2bp2* and *Igf2bp3* mRNA in *Lin28a* Tg muscle.

(E) Model of *Lin28*/*let-7* pathway in glucose metabolism. Error bars represent SEM. *$p < 0.05$, **$p < 0.01$.

et al., 2010). Given that *Lin28a/b* is downregulated in most tissues after embryogenesis, while *let-7* increases in adult tissues, lingering questions from our earlier report were first, whether *let-7* was sufficient to influence organismal growth, and second, what function does *let-7* have in adult physiology? Our observation that the *iLin28a*, *iLIN28B*, and *iLet-7* Tg gain of function mice, as well as muscle-specific *Lin28a* loss of function mice manifest complementary phenotypes supports the notion that *Lin28a/b* and *let-7* are both regulators of growth and developmental maturation. We propose that different developmental time-points demand distinct metabolic needs, and that global regulators such as *Lin28* temporally coordinate growth with metabolism. The dynamic relationship between *Lin28*, *let-7* and metabolic states during major growth milestones in mammals is reminiscent of the heterochronic mutant phenotypes originally defined in *C. elegans* (Ambros and Horvitz, 1984; Moss et al., 1997; Boehm and Slack, 2005), and suggests that metabolism, like differentiation, is temporally controlled.

Lin28a/b and *let-7* Influence Glucose Metabolism through the Insulin-PI3K-mTOR Pathway

We have shown that *Lin28a/b* and *let-7* regulates insulin-PI3K-mTOR signaling, a highly conserved pathway that regulates growth and glucose metabolism throughout evolution. PI3K/Akt signaling is known to promote Glut4 translocation to upregulate glucose uptake, while mTOR signaling can promote glucose uptake and glycolysis by changing gene expression independently of Glut4 translocation (Brugarolas et al., 2003; Buller et al., 2008; Duvel et al., 2010). Previous studies have shown that Lin28a directly promotes Igf2 (Polesskaya et al., 2007) and HMGA1 translation (Peng et al., 2011), and that *let-7* suppresses IGF1R translation in hepatocellular carcinoma cells (Wang et al., 2010). Consistent with these findings, our results define a model whereby *Lin28a/b* and *let-7* coordinately regulate the insulin-PI3K-mTOR pathway at multiple points (Figure 6E), a concept that is consistent with the hypotheses that miRNAs and RNA binding proteins regulate signaling pathways by tuning the production of a broad array of proteins rather than switching single components on or off (Kennell et al., 2008; Hatley et al., 2010; Small and Olson, 2011). Coordinated regulation is important because negative feedback loops exist within the insulin-PI3K-mTOR pathway. Loss-of-function and pharmacological inhibition studies have shown that the mTOR target S6K1, for instance, inhibits and desensitizes insulin-PI3K signaling by phosphorylating IRS1 protein and suppressing *IRS1* gene transcription (Harrington et al., 2004; Shah et al., 2004; Tremblay et al., 2007; Um et al., 2004). Conversely, TSC1-2 promotes insulin-PI3K signaling by suppressing mTOR signaling (Harrington et al., 2004; Shah et al., 2004). Although the effects of *let-7* and *Lin28a/b* on the expression of individual genes are modest, simultaneous regulation of multiple components such as *IGF2, IGF1R, INSR, IRS2, PIK3IP1, AKT2, TSC1, RICTOR* in the

insulin-PI3K-mTOR signaling pathway could explain how this RNA processing pathway coordinately regulates insulin sensitivity and glucose metabolism by effectively bypassing these negative feedback loops.

Whereas our work has implicated *let-7* as a regulator of insulin-PI3K-mTOR signaling, we do not exclude a parallel role for direct mRNA targets of Lin28a/b in glucose metabolism, a hypothesis supported by the recent findings that *HMGA1* is translationally regulated by LIN28A and mutated in 5%–10% of T2D patients (Peng et al., 2011; Chiefari et al., 2011). Such non-*let-7* functions are also suggested by the fact that muscle-specific loss of *Lin28a* results in glucose derangement without significant *let-7* changes. Nevertheless, it remains likely that during other developmental stages or in other tissues, *let-7* suppression by *Lin28a* or *Lin28b* is required for normal glucose homeostasis. The effects of the *Lin28*/*let-7* pathway on glucose metabolism in our murine models, together with our observation that genes regulated by *let-7* are associated with T2D risk in humans, indicates important functional roles for both *Lin28a/b* and *let-7* in human metabolism.

let-7 Targets Are Relevant to Disparate Human Diseases: Cancer and T2D

Metabolic reprogramming in malignancy is thought to promote a tumor's ability to produce biomass and tolerate stress in the face of uncertain nutrient supplies (Vander Heiden et al., 2009). During their rapid growth phase early in development, embryos may utilize similar programs to maintain a growth-permissive metabolism. Dissecting the genetic underpinnings of embryonic metabolism would likely provide important insights into the nutrient uptake programs that are co-opted in cancer. While loss of function studies in the early embryo would help define the metabolic roles of oncofetal genes in their physiologic context, classical in vivo metabolic assays are difficult to perform in embryos. *Lin28a* and *Lin28b* are oncofetal genes, and thus highly expressed in early embryogenesis and then silenced in most adult tissues, but reactivated in cancer (Yang and Moss, 2003; Viswanathan et al., 2009). Cancer cells may utilize the embryonic function of *Lin28a/b* to drive a metabolic shift toward increased glucose uptake and glycolysis – a phenomenon termed the "Warburg effect." Previously, we showed that *Lin28a* expression promotes glycolytic metabolism in muscle in vivo and in C2C12 myoblasts in vitro (Zhu et al., 2010). Though we cannot yet readily determine the metabolic effects of shutting off *Lin28a/b* within the embryo, we have dissected the potent effects of reactivating and inactivating this oncofetal program in adults. Conversely, in normal adult tissues that do not express high levels of *Lin28a* or *Lin28b*, one might ask if a role for the highly abundant *let-7* is to lock cells into the metabolism of terminally differentiated cells to prevent aberrant reactivation of embryonic metabolic programs. Further studies are required to understand how this pathway may link mechanisms of tumorigenesis and diabetogenesis.

Our report implicates *Lin28a/b* and *let-7* as important modulators of glucose metabolism through interactions with the insulin-PI3K-mTOR pathway and T2D-associated genes identified in GWAS. Although it is likely that additional mechanisms and feedback loops exist, our data suggests a model whereby *Lin28a/b* and *let-7* coordinate the GWAS identified genes and the insulin-PI3K-mTOR pathway to regulate glucose metabolism (Figure 6E). It also suggests that enhancing *Lin28* function or abrogating *let-7* may be therapeutically promising for diseases like obesity and diabetes. Likewise, results from this work might shed light on the physiology of aging and, specifically, how the accumulation of *let-7* in aging tissues may contribute to the systemic insulin resistance that accompanies aging.

EXPERIMENTAL PROCEDURES

Mice

All animal procedures were based on animal care guidelines approved by the Institutional Animal Care and Use Committee. Mouse lines used in this study are described in the Extended Experimental Procedures and Figure S5.

Indirect Calorimetry

The apparatus used was a set of 16 OxyMax® Metabolic Activity Monitoring chambers (Columbus Instruments; Columbus, OH, USA). Each chamber consisted of a self-contained unit capable of providing continuous measurements of an individual mouse's total activity and feeding behavior. Monitoring occurred over a 3-day period. Each subject was placed into an individual chamber on day 1, with free access to food and water during the course of the experiment. Subjects were maintained under a normal 12:12 hr light:dark cycle. All measurements were sampled periodically (at approximately 12 min intervals) and automatically recorded via the OXYMAX Windows V3.22 software. Activity measures over the final 24 hr period were parceled into 2-h bins and these were used to express diurnal activity levels.

Quantitative RT-PCR

Performed with standard methods, which are described in detail in the Extended Experimental Procedures.

Histology

Tissue samples were fixed in 10% buffered formalin or Bouin's solution and embedded in paraffin.

Glucose and Insulin Tolerance Tests

Overnight-fasted mice were given i.p. glucose (2 mg/g body weight). For insulin tolerance test, 5 hr fasted mice were given 0.75 U insulin/kg body weight by i.p. injection (Humulin). Blood glucose was determined with a Lifescan One Touch glucometer. Insulin levels were measured by ELISA (Crystal Chem).

Cloning

Murine *Lin28a* and human *LIN28B* cDNA was subcloned into pBabe.Puro and pMSCV.Neo retroviral vectors. *LIN28B* and Control shRNA in lentiviral plasmids were purchased from Sigma-Aldrich and previously reported in Viswanathan et al., 2009. UTR cloning for luciferase reporters is described in Table S2.

Cell Culture, Viral Production, and Transfection

Performed using standard methods as described in the Extended Experimental Procedures.

Glucose Uptake Assay

In vitro glucose uptake assays were performed as described in Berti and Gammeltoft, 1999.

Drug Treatments

Rapamycin was injected i.p. 3 times a week for mouse experiments. For cell culture, C2C12 myotubes differentiated for 3 days were incubated with inhibitors for 1 day prior to glucose uptake assays. See Extended Experimental Procedures for further details.

Western Blot Assay

Performed using standard methods. Detailed methods and reagents used are described in the Extended Experimental Procedures.

Luciferase Reporter Assay

10 ng of each construct was co-transfected with 10 nM miRNA duplexes or into HEK293T cells in a 96-well plate using lipofectamin-2000 (Invitrogen). After 48 hr, the cell extract was obtained; firefly and *Renilla* luciferase activities were measured with the Promega Dual-Luciferase® reporter system.

MAGENTA Analysis

See Results, Table 1 Legend, and Extended Experimental Procedures for detailed methods.

Statistical Analysis

Data is presented as mean ± SEM, and Student's t test (two-tailed distribution, two-sample unequal variance) was used to calculate *p* values. Statistical significance is displayed as $p < 0.05$ (one asterisk) or $p < 0.01$ (two asterisks). The tests were performed using Microsoft Excel where the test type is always set to two-sample equal variance.

SUPPLEMENTAL INFORMATION

Supplemental Information includes Extended Experimental Procedures, a list of DIAGRAM and MAGIC consortia members with affiliations, and five figures and can be found with this article online at doi:10.1016/j.cell.2011.08.033.

ACKNOWLEDGMENTS

We thank John Powers, Harith Rajagopalan, Jason Locasale, Abdel Saci, Akash Patnaik, Charles Kaufman, Christian Mosimann and Lewis Cantley for invaluable discussions and advice, Roderick Bronson and the Harvard Medical School Rodent Histopathology Core for mouse tissue pathology, and the Harvard Neurobehavior Laboratory for CLAMS experiments. This work was supported by grants from the US NIH to G.Q.D., a Graduate Training in Cancer Research Grant and a American Cancer Society Postdoctoral Fellowship to H.Z., the NSS Scholarship from the Agency for Science, Technology and Research, Singapore for N.S.C, an NIH NIDDK Diseases Career Development Award to M.G.K, and an American Diabetes Association Postdoctoral Fellowship for A.V.S. J.M.E. was supported by the National Human Genome Research Institute (NHGRI). R.I.G. was supported by US National Institute of General Medical Sciences (NIGMS) and is a Pew Research Scholar. D.A. is a Distinguished Clinical Scholar of the Doris Duke Charitable Foundation. G.Q.D. is a recipient of Clinical Scientist Awards in Translational Research from the Burroughs Wellcome Fund and the Leukemia and Lymphoma Society, and an investigator of the Howard Hughes Medical Institute and the Manton Center for Orphan Disease Research. H.Z. and N.S.C designed and performed the experiments, and wrote the manuscript. A.V.S. and D.A. performed bioinformatic analysis on *let-7* targets in GWAS. G.S. and S.P.S. performed expression analysis, metabolic assays and mouse husbandry. G.S., W.S.E. and A.T. generated the mouse strains. J.E.T, R.T. and R.I.G. assisted with the luciferase assays. J.P.H., R.I.G., G.S., and A.T generated the conditional knockout mice. M.G.K. helped to design the experiments. G.Q.D. designed and supervised experiments, and wrote the manuscript. The authors declare no competing financial interests.

Received: December 17, 2010
Revised: May 9, 2011
Accepted: August 5, 2011
Published: September 29, 2011

REFERENCES

Abbott, A.L., Alvarez-Saavedra, E., Miska, E.A., Lau, N.C., Bartel, D.P., Horvitz, H.R., and Ambros, V. (2005). The let-7 MicroRNA family members mir-48, mir-84, and mir-241 function together to regulate developmental timing in Caenorhabditis elegans. Dev. Cell *9*, 403–414.

Ambros, V., and Horvitz, H.R. (1984). Heterochronic mutants of the nematode Caenorhabditis elegans. Science *226*, 409–416.

Beard, C., Hochedlinger, K., Plath, K., Wutz, A., and Jaenisch, R. (2006). Efficient method to generate single-copy transgenic mice by site-specific integration in embryonic stem cells. Genesis *44*, 23–28.

Berti, L., and Gammeltoft, S. (1999). Leptin stimulates glucose uptake in C2C12 muscle cells by activation of ERK2. Mol. Cell. Endocrinol. *157*, 121–130.

Boehm, M., and Slack, F. (2005). A developmental timing microRNA and its target regulate life span in C. elegans. Science *310*, 1954–1957.

Boyerinas, B., Park, S.M., Shomron, N., Hedegaard, M.M., Vinther, J., Andersen, J.S., Feig, C., Xu, J., Burge, C.B., and Peter, M.E. (2008). Identification of let-7-regulated oncofetal genes. Cancer Res. *68*, 2587–2591.

Brugarolas, J.B., Vazquez, F., Reddy, A., Sellers, W.R., and Kaelin, W.G., Jr. (2003). TSC2 regulates VEGF through mTOR-dependent and -independent pathways. Cancer Cell *4*, 147–158.

Buller, C.L., Loberg, R.D., Fan, M.H., Zhu, Q., Park, J.L., Vesely, E., Inoki, K., Guan, K.L., and Brosius, F.C., 3rd. (2008). A GSK-3/TSC2/mTOR pathway regulates glucose uptake and GLUT1 glucose transporter expression. Am J Physiol Cell Physiol *295*, C836–843.

Chiefari, E., Tanyolac, S., Paonessa, F., Pullinger, C.R., Capula, C., Iiritano, S., Mazza, T., Forlin, M., Fusco, A., Durlach, V., et al. (2011). Functional variants of the HMGA1 gene and type 2 diabetes mellitus. J. Am. Med. Assoc. *305*, 903–912.

Denko, N.C. (2008). Hypoxia, HIF1 and glucose metabolism in the solid tumour. Nat. Rev. Cancer *8*, 705–713.

Dupuis, J., Langenberg, C., Prokopenko, I., Saxena, R., Soranzo, N., Jackson, A.U., Wheeler, E., Glazer, N.L., Bouatia-Naji, N., Gloyn, A.L., et al. (2010). New genetic loci implicated in fasting glucose homeostasis and their impact on type 2 diabetes risk. Nat. Genet. *42*, 105–116.

Duvel, K., Yecies, J.L., Menon, S., Raman, P., Lipovsky, A.I., Souza, A.L., Triantafellow, E., Ma, Q., Gorski, R., Cleaver, S., et al. (2010). Activation of a metabolic gene regulatory network downstream of mTOR complex 1. Mol. Cell *39*, 171–183.

Engelman, J.A., Luo, J., and Cantley, L.C. (2006). The evolution of phosphatidylinositol 3-kinases as regulators of growth and metabolism. Nat. Rev. Genet. *7*, 606–619.

Gao, P., Tchernyshyov, I., Chang, T.C., Lee, Y.S., Kita, K., Ochi, T., Zeller, K.I., De Marzo, A.M., Van Eyk, J.E., Mendell, J.T., et al. (2009). c-Myc suppression of miR-23a/b enhances mitochondrial glutaminase expression and glutamine metabolism. Nature *458*, 762–765.

Grimson, A., Farh, K.K., Johnston, W.K., Garrett-Engele, P., Lim, L.P., and Bartel, D.P. (2007). MicroRNA targeting specificity in mammals: determinants beyond seed pairing. Mol. Cell *27*, 91–105.

Guertin, D.A., and Sabatini, D.M. (2007). Defining the role of mTOR in cancer. Cancer Cell *12*, 9–22.

Guo, Y., Chen, Y., Ito, H., Watanabe, A., Ge, X., Kodama, T., and Aburatani, H. (2006). Identification and characterization of lin-28 homolog B (LIN28B) in human hepatocellular carcinoma. Gene *384*, 51–61.

Harrington, L.S., Findlay, G.M., Gray, A., Tolkacheva, T., Wigfield, S., Rebholz, H., Barnett, J., Leslie, N.R., Cheng, S., Shepherd, P.R., et al. (2004). The TSC1-2 tumor suppressor controls insulin-PI3K signaling via regulation of IRS proteins. J. Cell Biol. *166*, 213–223.

Hatley, M.E., Patrick, D.M., Garcia, M.R., Richardson, J.A., Bassel-Duby, R., van Rooij, E., and Olson, E.N. (2010). Modulation of K-Ras-dependent lung tumorigenesis by MicroRNA-21. Cancer Cell *18*, 282–293.

Heo, I., Joo, C., Cho, J., Ha, M., Han, J., and Kim, V.N. (2008). Lin28 mediates the terminal uridylation of let-7 precursor MicroRNA. Mol Cell *32*, 276–284.

Hyun, S., Lee, J.H., Jin, H., Nam, J., Namkoong, B., Lee, G., Chung, J., and Kim, V.N. (2009). Conserved MicroRNA miR-8/miR-200 and its target USH/FOG2 control growth by regulating PI3K. Cell *139*, 1096–1108.

Johnson, S.M., Grosshans, H., Shingara, J., Byrom, M., Jarvis, R., Cheng, A., Labourier, E., Reinert, K.L., Brown, D., and Slack, F.J. (2005). RAS is regulated by the let-7 microRNA family. Cell *120*, 635–647.

Kennell, J.A., Gerin, I., MacDougald, O.A., and Cadigan, K.M. (2008). The microRNA miR-8 is a conserved negative regulator of Wnt signaling. Proc. Natl. Acad. Sci. USA *105*, 15417–15422.

Kumar, M.S., Erkeland, S.J., Pester, R.E., Chen, C.Y., Ebert, M.S., Sharp, P.A., and Jacks, T. (2008). Suppression of non-small cell lung tumor development by the let-7 microRNA family. Proc Natl Acad Sci USA *105*, 3903–3908.

Laplante, M., and Sabatini, D.M. (2009). An emerging role of mTOR in lipid biosynthesis. Curr. Biol. *19*, R1046–R1052.

Lee, Y., and Dutta, A. (2007). The tumor suppressor microRNA let-7 represses the HMGA2 oncogene. Genes & Development *21*, 1025–1030.

Legesse-Miller, A., Elemento, O., Pfau, S.J., Forman, J.J., Tavazoie, S., and Coller, H.A. (2009). let-7 Overexpression leads to an increased fraction of cells in G2/M, direct down-regulation of Cdc34, and stabilization of Wee1 kinase in primary fibroblasts. J. Biol. Chem. *284*, 6605–6609.

Lu, L., Katsaros, D., de la Longrais, I.A., Sochirca, O., and Yu, H. (2007). Hypermethylation of let-7a-3 in epithelial ovarian cancer is associated with low insulin-like growth factor-II expression and favorable prognosis. Cancer Res. *67*, 10117–10122.

Mayr, C., Hemann, M.T., and Bartel, D.P. (2007). Disrupting the pairing between let-7 and Hmga2 enhances oncogenic transformation. Science *315*, 1576–1579.

Moss, E.G., Lee, R.C., and Ambros, V. (1997). The cold shock domain protein LIN-28 controls developmental timing in C. elegans and is regulated by the lin-4 RNA. Cell *88*, 637–646.

Newman, M.A., Thomson, J.M., and Hammond, S.M. (2008). Lin-28 interaction with the Let-7 precursor loop mediates regulated microRNA processing. RNA *14*, 1539–1549.

Nimmo, R.A., and Slack, F.J. (2009). An elegant miRror: microRNAs in stem cells, developmental timing and cancer. Chromosoma *118*, 405–418.

Peng, S., Chen, L.L., Lei, X.X., Yang, L., Lin, H., Carmichael, G.G., and Huang, Y. (2011). Genome-wide studies reveal that lin28 enhances the translation of genes important for growth and survival of human embryonic stem cells. Stem Cells *29*, 496–504.

Peter, M. (2009). Let-7 and miR-200 microRNAs: Guardians against pluripotency and cancer progression. Cell Cycle. *8*, 843–852.

Piskounova, E., Viswanathan, S.R., Janas, M., LaPierre, R.J., Daley, G.Q., Sliz, P., and Gregory, R.I. (2008). Determinants of microRNA processing inhibition by the developmentally regulated RNA-binding protein Lin28. J. Biol. Chem. *283*, 21310–21314.

Polesskaya, A., Cuvellier, S., Naguibneva, I., Duquet, A., Moss, E.G., and Harel-Bellan, A. (2007). Lin-28 binds IGF-2 mRNA and participates in skeletal myogenesis by increasing translation efficiency. Genes & Development *21*, 1125–1138.

Reinhart, B.J., Slack, F.J., Basson, M., Pasquinelli, A.E., Bettinger, J.C., Rougvie, A.E., Horvitz, H.R., and Ruvkun, G. (2000). The 21-nucleotide let-7 RNA regulates developmental timing in Caenorhabditis elegans. Nature *403*, 901–906.

Rybak, A., Fuchs, H., Smirnova, L., Brandt, C., Pohl, E.E., Nitsch, R., and Wulczyn, F.G. (2008). A feedback loop comprising lin-28 and let-7 controls pre-let-7 maturation during neural stem-cell commitment. Nat. Cell Biol. *10*, 987–993.

Segrè, A.V., DIAGRAM Consortium, MAGIC investigators, Groop, L., Mootha, V.K., Daly, M.J., and Altshuler, D. (2010). Common inherited variation in mitochondrial genes is not enriched for associations with type 2 diabetes or related glycemic traits. PLoS Genet *6*, e1001058.

Selbach, M., Schwanhausser, B., Thierfelder, N., Fang, Z., Khanin, R., and Rajewsky, N. (2008). Widespread changes in protein synthesis induced by microRNAs. Nature *455*, 58–63.

Shah, O.J., Wang, Z., and Hunter, T. (2004). Inappropriate activation of the TSC/Rheb/mTOR/S6K cassette induces IRS1/2 depletion, insulin resistance, and cell survival deficiencies. Curr. Biol. *14*, 1650–1656.

Small, E.M., and Olson, E.N. (2011). Pervasive roles of microRNAs in cardiovascular biology. Nature *469*, 336–342.

Tremblay, F., Brule, S., Hee Um, S., Li, Y., Masuda, K., Roden, M., Sun, X.J., Krebs, M., Polakiewicz, R.D., Thomas, G., et al. (2007). Identification of IRS-1 Ser-1101 as a target of S6K1 in nutrient- and obesity-induced insulin resistance. Proc. Natl. Acad. Sci. USA *104*, 14056–14061.

Um, S.H., Frigerio, F., Watanabe, M., Picard, F., Joaquin, M., Sticker, M., Fumagalli, S., Allegrini, P.R., Kozma, S.C., Auwerx, J., et al. (2004). Absence of S6K1 protects against age- and diet-induced obesity while enhancing insulin sensitivity. Nature *431*, 200–205.

Vander Heiden, M.G., Cantley, L.C., and Thompson, C.B. (2009). Understanding the Warburg effect: the metabolic requirements of cell proliferation. Science *324*, 1029–1033.

Viswanathan, S.R., and Daley, G.Q. (2010). Lin28: A microRNA regulator with a macro role. Cell *140*, 445–449.

Viswanathan, S.R., Daley, G.Q., and Gregory, R.I. (2008). Selective blockade of microRNA processing by Lin28. Science *320*, 97–100.

Viswanathan, S.R., Powers, J.T., Einhorn, W., Hoshida, Y., Ng, T.L., Toffanin, S., O'Sullivan, M., Lu, J., Phillips, L.A., Lockhart, V.L., et al. (2009). Lin28 promotes transformation and is associated with advanced human malignancies. Nat. Genet. *41*, 843–848.

Voight, B.F., Scott, L.J., Steinthorsdottir, V., Morris, A.P., Dina, C., Welch, R.P., Zeggini, E., Huth, C., Aulchenko, Y.S., Thorleifsson, G., et al. (2010). Twelve type 2 diabetes susceptibility loci identified through large-scale association analysis. Nat. Genet. *42*, 579–589.

Wang, Y.C., Chen, Y.L., Yuan, R.H., Pan, H.W., Yang, W.C., Hsu, H.C., and Jeng, Y.M. (2010). Lin-28B expression promotes transformation and invasion in human hepatocellular carcinoma. Carcinogenesis *31*, 1516–1522.

Xu, B., and Huang, Y. (2009). Histone H2a mRNA interacts with Lin28 and contains a Lin28-dependent posttranscriptional regulatory element. Nucleic Acids Res. *37*, 4256–4263.

Xu, B., Zhang, K., and Huang, Y. (2009). Lin28 modulates cell growth and associates with a subset of cell cycle regulator mRNAs in mouse embryonic stem cells. RNA *15*, 357–361.

Yang, D.H., and Moss, E.G. (2003). Temporally regulated expression of Lin-28 in diverse tissues of the developing mouse. Gene Expr Patterns *3*, 719–726.

Yun, J., Rago, C., Cheong, I., Pagliarini, R., Angenendt, P., Rajagopalan, H., Schmidt, K., Willson, J.K., Markowitz, S., Zhou, S., et al. (2009). Glucose deprivation contributes to the development of KRAS pathway mutations in tumor cells. Science *325*, 1555–1559.

Zhu, H., Shah, S., Shyh-Chang, N., Shinoda, G., Einhorn, W.S., Viswanathan, S.R., Takeuchi, A., Grasemann, C., Rinn, J.L., Lopez, M.F., et al. (2010). Lin28a transgenic mice manifest size and puberty phenotypes identified in human genetic association studies. Nat. Genet. *42*, 626–630.

Cell

EXTENDED EXPERIMENTAL PROCEDURES

Mice

Flag-tagged mouse *Lin28a* and human *LIN28B* open reading frames were cloned into pBS plasmid (Figure S5A). The engineered *let-7* miRNA, *let-7S21L*, (Piskounova et al., 2008) was also cloned into pBS31 plasmid (Figure S5A). Targeting was performed into V6.5 ES cells containing *M2-rtTA* targeted to the *Rosa26* locus, as previously described (Beard et al., 2006). Design of conditional *Lin28a* knockout mice is shown in Figure S5B–D. For all strains, chimeric mice were generated by injection of ES cells into Balb/c blastocysts, then bred to CD-1 females to generate germline-transmitted pups. The line was maintained on the CD-1 background and the C57/B6 background by backcrossing > 5 times. For all experiments, littermate controls were used.

Cell Culture, Viral Production, and Transfection

For ecotropic viral production, retroviral plasmid DNA and pCL-Eco were transfected into 293T cells in a 1:1 mass ratio and virus harvested after 48h. For VSV-G pseudotyped lentivirus, viral plasmid, lentiviral gag/pol, and VSV-G were transfected in a mass ratio 1:0.9:0.1, and virus was harvested after 72 hr. 1 ml of unconcentrated viral supernatant was used to infect 50,000 cells. Infected cells were selected on antibiotic prior to subsequent analysis. C2C12, mouse NIH 3T3, human HEK293T cells were maintained in DMEM media, supplemented with 10% fetal bovine serum (FBS) and 1% Pen-Strep (Invitrogen). C2C12 myoblasts were maintained at subconfluent densities. For C2C12 differentiation to myotubes, cells were grown to confluency and the media was switched to DMEM with 2% horse serum and 1% Pen-Strep. *let-7a/f* and the negative control *cel-miR-67* miRNA duplexes and antisense oligonucleotides (Dharmacon) were transfected at a final concentration of 40 nM in C2C12 myoblasts and 10 nM in all other cells.

Quantitative RT-PCR

RNA was collected using Trizol® reagent (Invitrogen). For qRT-PCR of miRNAs, 100 ng of total RNA was reverse-transcribed and subjected to Taqman® miRNA assay (Applied Biosystems). For qRT-PCR of mRNAs, cDNA synthesis was performed with 1 μg of total RNA using SuperScript II and random hexamer primers (Invitrogen). The expression of all genes was analyzed by SYBR® Green assays (Applied Biosystems) using qSTAR® qPCR primers (OriGene) and the Stratagene real-time PCR system. mRNA and miRNA expression was measured by quantitative PCR using the Delta-Delta CT method.

Western Blot Assay

Cells were lysed in RIPA buffer (Pierce). Proteins was separated by a 10% polyacrylamide gel and transferred to a methanol-activated PVDF membrane (GE Healthcare). The membrane was blocked for one hour in PBST containing 5% milk and subsequently probed with primary antibodies overnight at 4°C. After 1 hr incubation with sheep-anti-mouse or donkey-anti-rabbit HRP-conjugated secondary antibody (GE Healthcare), the protein level was detected with SuperSignal West Pico and Femto Luminol reagents (Thermo Scientific). Antibodies used were anti-IGF1R (ab39675, Abcam), anti-IRS2 (#3089, Cell Signaling), anti-insulin receptor beta (#3025, Cell Signaling), anti-pan-Akt (#4691, Cell Signaling), anti-phospho-Akt (Ser473; #4060, Cell Signaling), anti-phospho-Akt (Thr308; #2965, Cell Signaling), anti-rpS6 (#2317, Cell Signaling), anti-phospho-rpS6 (Ser235/236; #2211, Cell Signaling), anti-4EBP1 (#9644, Cell Signaling), anti-phospho-4EBP1 (Thr37/46, #2855, Cell Signaling), anti-Rictor (#2114, Cell Signaling), anti-Raptor (#2280, Cell Signaling), anti-alpha tubulin (#3873, Cell Signaling), anti-beta actin (ab8226, Abcam), anti-IGF2BP1/2/3 (sc-33594, Santa Cruz), anti-Lin28a (#3978, Cell Signaling), and anti-LIN28B (#4196, Cell Signaling).

Drug Treatments

Rapamycin (LC Laboratories) was dissolved in 100% ethanol, diluted in vehicle solution (0.25% Tween 80, 0.25% PEG-400 in PBS), and a dose of 4 mg/kg mouse weight was injected intraperitoneally 3 times a week for 4 weeks starting at P14. For cell culture, C2C12 myotubes differentiated for 3 days were incubated in rapamycin (20 ng/mL in DMSO), PD98059 (10 μM in DMSO; Calbiochem) or LY294002 (10 μM in DMSO; Calbiochem) for 1 day prior to glucose uptake assays. C2C12 myoblasts starved in 0% FBS media for 18 hr were pre-incubated with rapamycin (20 ng/mL in DMSO) or PD98059 (10 μM in DMSO; Calbiochem) for 1 hr before insulin stimulation (10 μg/mL; Sigma) for 10 min, prior to lysis for Western blot analysis.

MAGENTA GWAS Analysis

Gene set enrichment analysis of *let-7* target gene associations with T2D and fasting glucose blood levels was conducted with MAGENTA as described in (Segrè et al., 2010). The enrichment *p*-value was computed for each *let-7* target gene set by comparing its enrichment score to a null distribution of 10,000 to 10^6 permuted gene sets of identical size randomly sampled from all genes in the genome. The 75^{th} percentile of all gene association *p*-values in the genome, adjusted for gene size, SNP density and LD properties, was used for the gene set enrichment cutoff. Genome-wide DNA variant association data were taken from DIAGRAM+ (Voight et al., 2010) and MAGIC (Dupuis et al., 2010) GWAS meta-analyses.

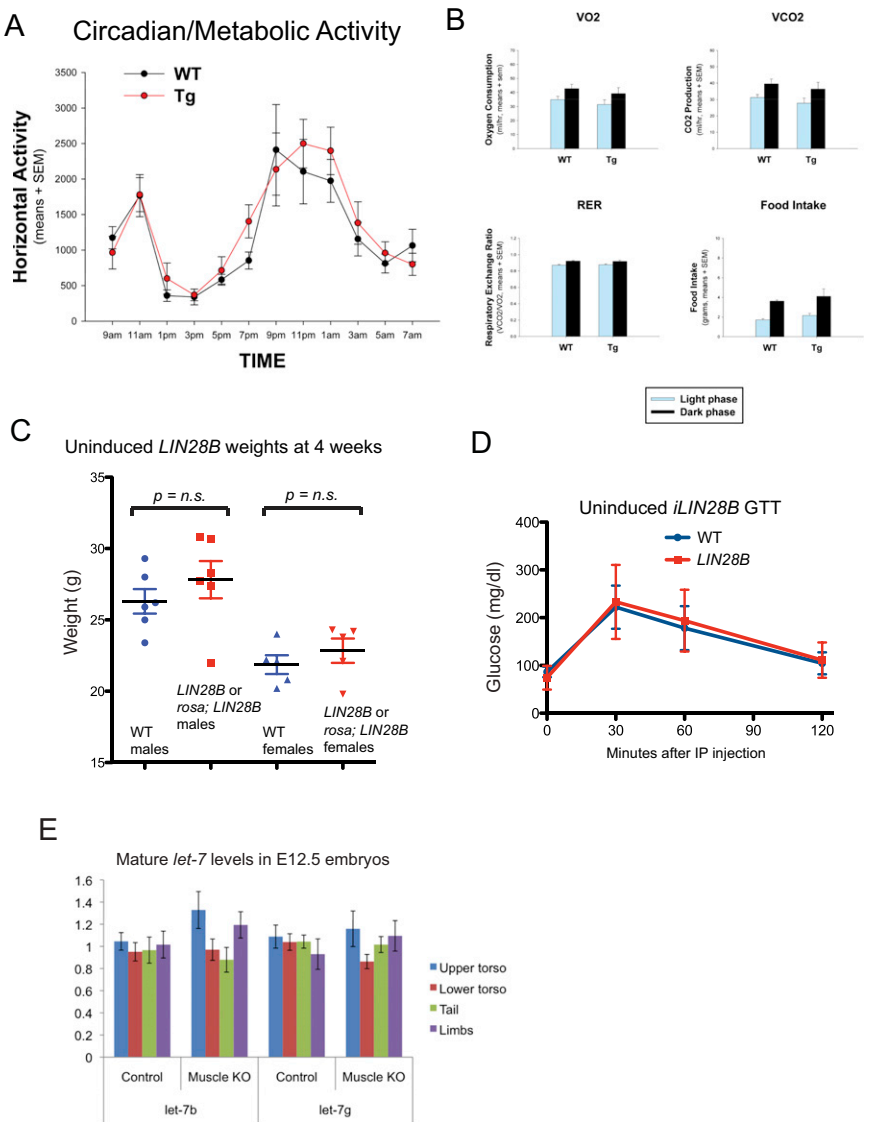

Figure S1. Further Characterization of *Lin28a/b* Gain and Loss of Function Mice, Related to Figure 1

Over 96 hr, there were no horizontal activity (A), O2/CO2 exchange, or food/water intake (B) differences between wild-type and *Lin28a* Tg mice.

(C) Weight and (D) GTT of uninduced wild-type and *LIN28B* Tg containing mice.

(E) Mature *let-7* miRNA expression in E12.5 wild-type and *Lin28a* muscle-specific knockout embryos. Error bars represent SEM. *p < 0.05, *p < 0.01.

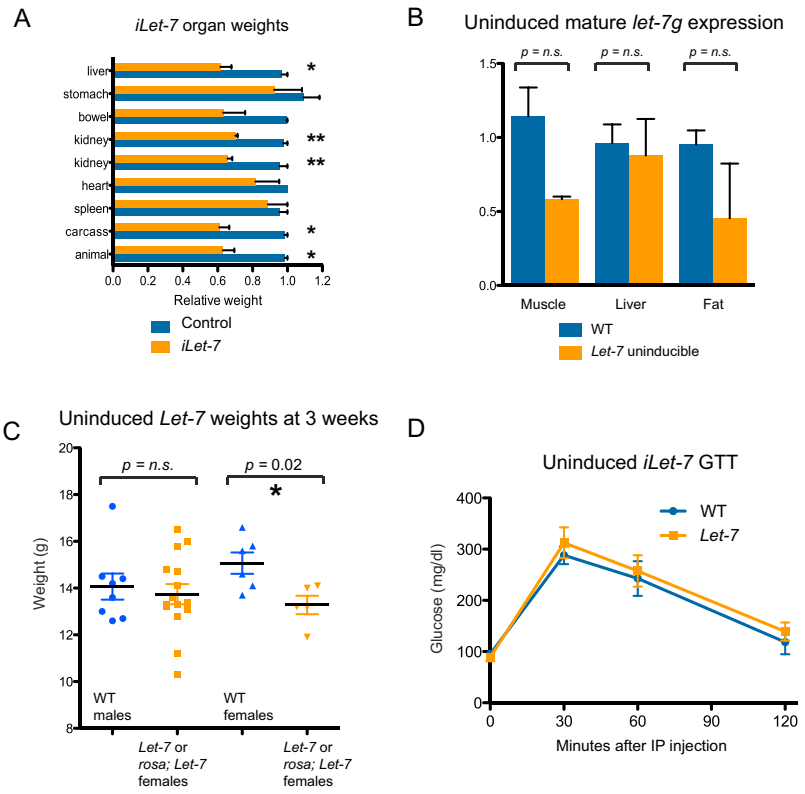

Figure S2. Further Characterization of *iLet-7* Transgenic Mice, Related to Figure 2

(A) Relative organ weights of *iLet-7* mice induced for 8 weeks.

(B) Mature *let-7g* expression in tissues of uninduced *iLet-7* or *Let-7* Tg carrying mice.

(C) Weight and (D) GTT of uninduced wild-type and *iLet-7* Tg containing mice. Error bars represent SEM. *$p < 0.05$, **$p < 0.01$.

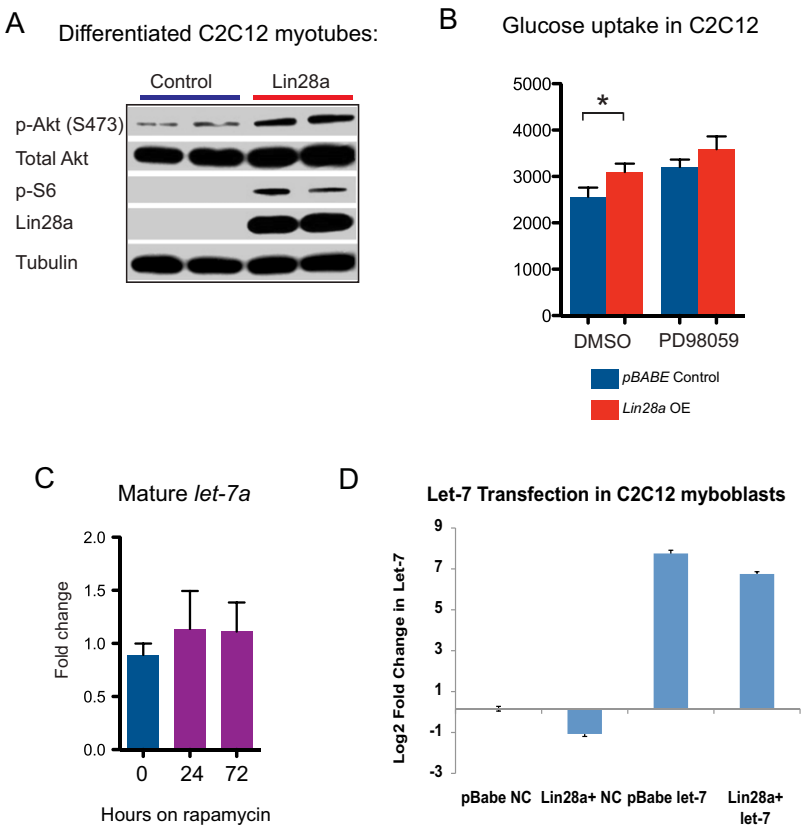

Figure S3. *Lin28a* Increases PI3K-mTOR Signaling in Differentiated Myotubes, the MAPK/Erk Inhibitor Does Not Abrogate *Lin28a*-Induced Glucose Uptake, and Rapamycin Does Not Alter *let-7* Levels in Myoblasts, Related to Figure 3

(A) Western blot showing Akt and S6 phosphorylation in C2C12 cells differentiated into myotubes for 3 days, expressing either *Lin28a* or the pBabe empty vector.

(B) Glucose uptake in 3-day-differentiated C2C12 myotubes after 24 hr treatment with 10 μM of the MAPK/Erk inhibitor PD98059, or DMSO.

(C) Effect of rapamycin on mature *let-7a* levels in C2C12 myoblasts.

(D) Mature *let-7* miRNA expression in C2C12 myoblasts. NC = negative control. Error bars represent SEM. *$p < 0.05$, **$p < 0.01$.

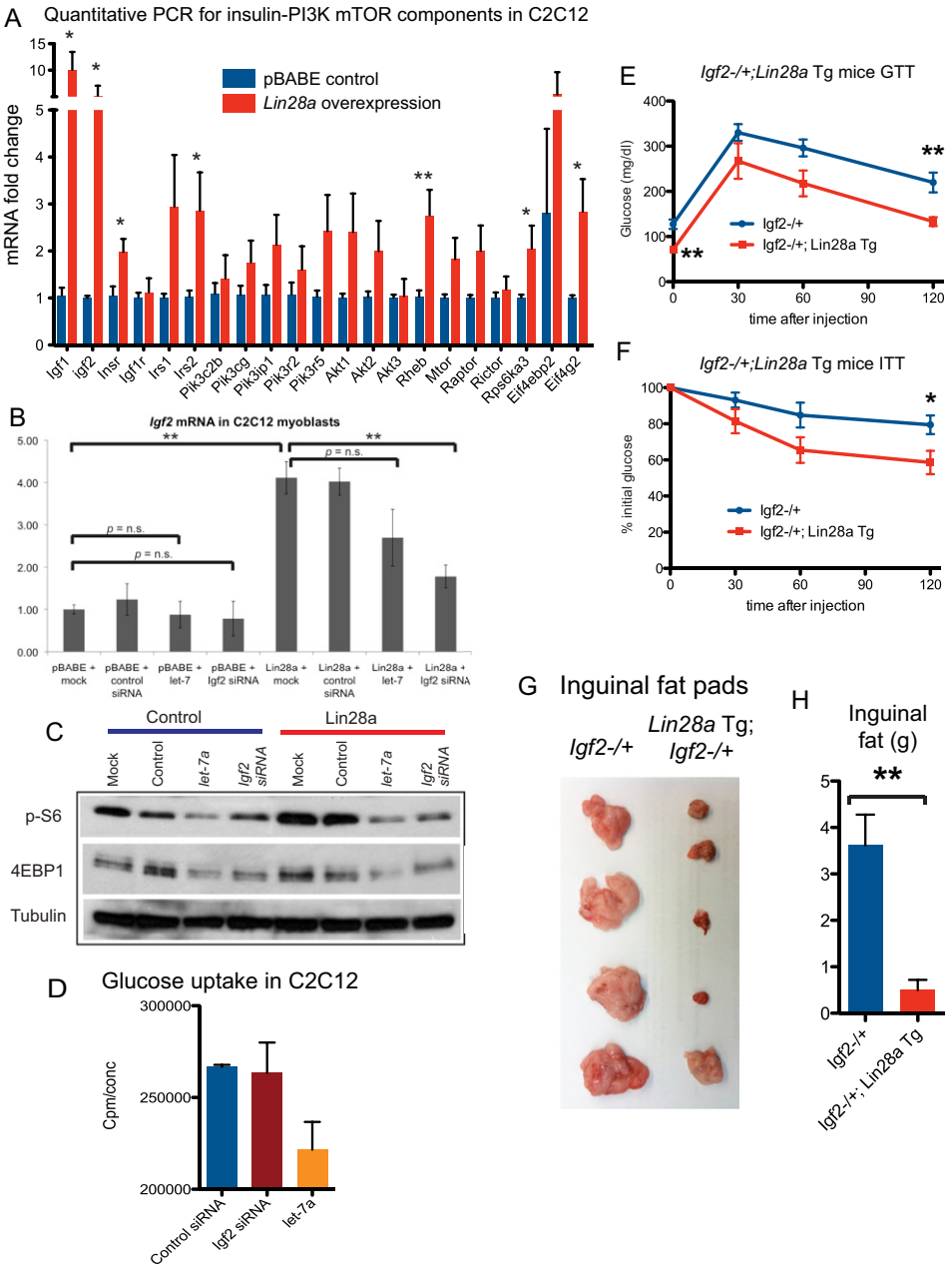

Figure S4. *Lin28a* Promotes Insulin-PI3K-mTOR Pathway Genes and *Igf2* Is Dispensable for *Lin28a's* Functions In Vitro and In Vivo

(A) Quantitative PCR for components of the insulin-PI3K-mTOR signaling pathway in C2C12 myoblasts, normalized to *Gapdh*, after *Lin28a* overexpression.

(B) *Igf2* mRNA expression in C2C12 myoblasts.

(C) S6 and 4EBP1 phosphorylation in C2C12 myoblasts after overexpression of *let-7a* and knockdown of *Igf2.*

(D) Glucose uptake in 3-day-differentiated C2C12 myotubes after siRNA knockdown of *Igf2* and overexpression of *let-7a* duplex.

(E) GTT and (F) ITT of *Igf2*-/+; *Lin28a* Tg versus *Igf2*-/+ mice. Since *Igf2* is imprinted and silenced on the maternal allele, all of the heterozygous offspring (labeled *Igf2*-/+) of a homozygous null father are functionally *Igf2* null.

(G) Inguinal fat pads dissected from 1-year-old *Igf2*-/+*; Lin28a Tg* and *Igf2*-/+ mice.

(H) Weight in grams of these fat pads. Error bars represent SEM. *p < 0.05, **p < 0.01.

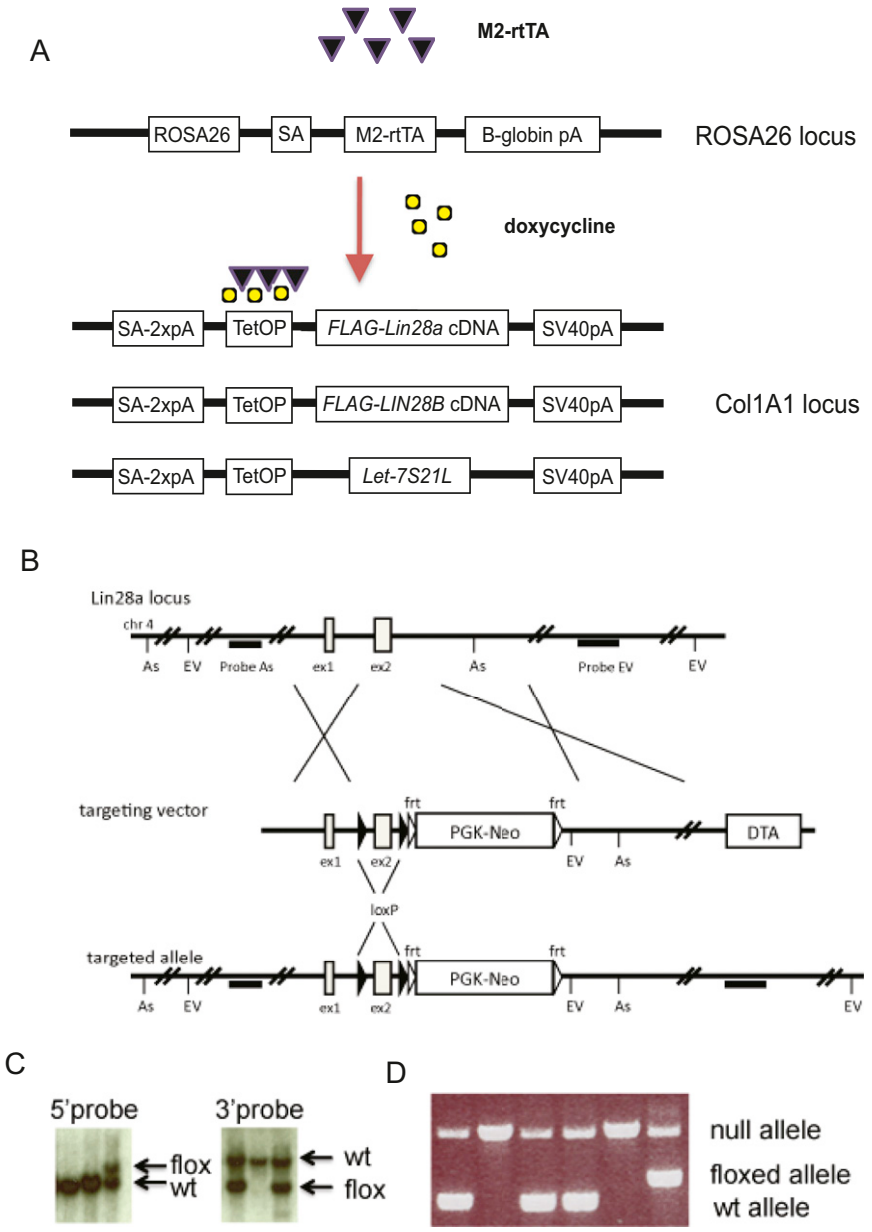

Figure S5. Constructs Used to Make Inducible Transgenic and Conditional Knockout Mice, Related to the Experimental Procedures

(A) Tetracycline inducible mouse constructs for *iLin28a, iLIN28B, and iLet-7* mice.

(B) Design of conditional *Lin28a* knockout mice. Upper: Genomic map of the *Lin28a* locus shows exons, restriction sites. Middle: *Lin28a* conditional targeting construct. Exon 2 is flanked by loxP sites. PGK-Neo cassette is flanked by a frt site. Lower: Targeted allele following a homologous recombination. As = Asp718, EV = EcoRV.

(C) Southern blot showing ESC clones with the floxed allele.

(D) PCR genotyping showing wild-type (wt), floxed and deleted (null) alleles.